Surface ozone-meteorology relationships: Spatial variations and the role of the jet stream

Gaige Hunter Kerr[1*], Darryn W. Waugh[1,2], Stephen D. Steenrod[3,4], Sarah A. Strode[3,4], and Susan E. Strahan[3,4]

[1]Department of Earth and Planetary Sciences, Johns Hopkins University, Baltimore, Maryland, USA
[2]School of Mathematics and Statistics, University of New South Wales, Sydney, New South Wales, Australia
[3]NASA Goddard Space Flight Center, Greenbelt, Maryland, USA
[4]Universities Space Research Association, GESTAR, Columbia, Maryland, USA

Key Points:

- The relationships among summertime O_3, temperature, and humidity vary over the Northern Hemisphere
- Daily variations in meteorology drive the O_3-meteorology covariance
- The jet impacts meridional flow, which acts on the latitudinal O_3 gradient and leads to variations in the O_3-meteorology relationships

[*]now at Department of Environmental and Occupational Health, George Washington University, Washington, DC, USA

Corresponding author: G. H. Kerr, `gaigekerr@gwu.edu`

Abstract

We investigate the relationships among summertime ozone (O_3), temperature, and humidity on daily timescales across the Northern Hemisphere using observations and model simulations. Temperature and humidity are significantly positively correlated with O_3 across continental regions in the mid-latitudes ($\sim 35-60°$N). Over the oceans, the relationships are consistently negative. For continental regions outside the mid-latitudes, the O_3-meteorology correlations are mixed in strength and sign but generally weak. Over some high latitude, low latitude, and marine regions, temperature and humidity are significantly anticorrelated with O_3. Daily variations in transport patterns linked to the position and meridional movement of the jet stream drive the relationships among O_3, temperature, and humidity. Within the latitudinal range of the jet, there is an increase (decrease) in O_3, temperature, and humidity over land with poleward (equatorward) movement of the jet, while over the oceans poleward movement of the jet results in decreases of these fields. Beyond the latitudes where the jet traverses, the meridional movement of the jet stream has variable or negligible effects on surface-level O_3, temperature, and humidity. The O_3-meteorology relationships are largely the product of the jet-induced changes in the surface-level meridional flow acting on the background meridional O_3 gradient. Our results underscore the importance of considering the role of the jet stream and surface-level flow for the O_3-meteorology relationships, especially in light of expected changes to these features under climate change.

Plain Language Summary

The relationship of ozone (O_3) with meteorological variables such as temperature and humidity at the earth's surface varies in strength and sign. Some regions, such as continental parts of the mid-latitudes, experience increases in O_3 as the temperature or humidity rises. However, this is not the case over the entire Northern Hemisphere. We use detailed computer simulations of atmospheric chemistry to show that these relationships are primarily the result of changes in meteorology, not changes in emissions or chemistry. The relationship between O_3 and meteorological variables is related to the north-south movement of the jet stream, powerful eastward-flowing air currents located near the tropopause that can encircle the hemisphere. Specifically, we find that the jet stream influences the O_3-meteorology relationships due to its effect on the north- and southward advection of O_3, temperature, and humidity and not due to cyclones and the associated frontal activity, as has been previously suggested. Our results are relevant for understanding the present-day O_3-meteorology relationships and how climate change may impact O_3 pollution.

1 Introduction

Ambient surface-level ozone (O_3) plays a prominent role in atmospheric chemistry (Fiore et al., 2015; Pusede et al., 2015), while posing significant threats to human health (Landrigan et al., 2018) and ecosystem productivity (Tai & Martin, 2017). Long-term trends in observed O_3 in the Northern Hemisphere mid-latitudes reveal sustained, year-round increases in baseline O_3 concentrations (Parrish et al., 2012), underpinning the need for a better understanding of the drivers of O_3 variability. Meteorology strongly affects O_3 concentrations and chemistry through both variations in prevailing weather conditions on daily, seasonal, or interannual timescales as well as long-terms trends associated with climate change (e.g., Jacob & Winner, 2009; Fiore et al., 2015; Otero et al., 2016; Lefohn et al., 2018). The meteorological, or transport-related, phenomena that affect O_3 are not cause-and-effect relationships in the same sense as emissions or chemical kinetics and energetics (i.e., temperature-dependent reaction or emissions rates). Rather, the link between O_3 and meteorology reflects a joint association (e.g., high temperatures are often associated with slow-moving anticyclones).

Previous studies have focused on characterizing the relationship between O_3 and temperature or humidity in historical data. Generally these studies found a positive O_3-temperature relationship (e.g., Rasmussen et al., 2012, 2013; Pusede et al., 2015) and a variable O_3-humidity relationship with substantial latitudinal variability (e.g., Camalier et al., 2007; Tawfik & Steiner, 2013; Kavassalis & Murphy, 2017). However, the majority of past studies on the O_3-meteorology relationships focused on populated, industrialized portions of the Northern Hemisphere mid-latitudes, potentially overlooking important variations of these relationships elsewhere. These studies have been conducted for different and often non-overlapping time periods during which changes of O_3 precursors could affect chemical background conditions (Kim et al., 2006; Derwent et al., 2010; Cooper et al., 2012; Simon et al., 2015; Lin et al., 2017). Finally, past studies have used different methodologies (e.g., O_3-relationships derived from hourly, daily, or seasonal data; see Brown-Steiner et al. (2015) for additional information). All these factors complicate direct comparisons from study to study; thus, it is difficult to piece together a comprehensive sense of how the O_3-meteorology relationships vary across the globe and what processes drive these relationships. Recent work by Kerr et al. (2019) and Porter and Heald (2019) suggests that greater than 50% of the covariance of O_3 and temperature in the United States (U.S.) and Europe on daily timescales stems from meteorological phenomena, not chemistry or emissions. It is an open question whether this also holds for the O_3-humidity relationship.

There have been several meteorological mechanisms proposed to link O_3 with temperature and humidity. However, little consensus exists as to which mechanism is the most important and the regions or timescales over which it operates. Baroclinic cyclones can disperse built-up concentrations of pollution by entraining polluted air from the planetary boundary layer (PBL) into the free troposphere (e.g., Mickley, 2004; Leibensperger et al., 2008; Knowland et al., 2015, 2017). Quasi-stationary anticyclones such as the Bermuda High can influence regional climate and O_3 (e.g., Zhu & Liang, 2013). Properties of the PBL, such as its height, or temperature inversions and mixing within the PBL, have also been suggested as transport-related mechanisms that affect surface-level O_3 (e.g., Dawson et al., 2007; He et al., 2013; Reddy & Pfister, 2016; Barrett et al., 2019). Winds near the earth's surface or aloft can ventilate pollution away from its source region (e.g., Camalier et al., 2007; Hegarty et al., 2007; Tai et al., 2010; Sun et al., 2017). Interactions among the atmosphere, land surface, and biosphere have been proposed to explain the O_3-humidity relationship in North America (Tawfik & Steiner, 2013; Kavassalis & Murphy, 2017). The jet stream is a pronounced feature of the general circulation of atmosphere in both the Northern and Southern Hemisphere mid-latitudes and is characterized by a region of strong eastward wind aloft. Its existence arises from momentum and heat fluxes forced by transient eddies, and the jet extends throughout the depth of the troposphere (Woollings et al., 2010). The variability of surface-level summertime O_3 as well as its relationship with temperature have been linked to the latitude of the jet stream over eastern North America (Barnes & Fiore, 2013; Shen et al., 2015). Similar connections between the jet position, persistence of the jet in a given position, and wintertime particulate matter with a diameter $< 2.5\ \mu$m ($PM_{2.5}$) have also been demonstrated in Europe (Ordóñez et al., 2019).

The aim of this paper is to document the relationships of surface-level temperature and specific humidity (henceforth "humidity") with O_3 in the Northern Hemisphere during boreal summer and explore the processes responsible for spatial variations of these relationships. Through our model simulations, we demonstrate that variations in transport-related processes drive the covariance of O_3 with temperature and humidity on daily timescales. We build off of the previous regionally-focused work of Barnes and Fiore (2013), Shen et al. (2015), and Ordóñez et al. (2019) to show the connections between the position of the jet stream and surface-level temperature, humidity, and O_3 variability hold across the Northern Hemisphere. Finally, we develop and test hypotheses that tie the jet stream to the surface-level relationships among O_3, temperature, and humidity.

2 Data and Methodology

2.1 Model Simulations

The majority of our analysis of the O_3-meteorology relationships is performed using simulations of NASA's Global Modeling Initiative chemical transport model (GMI CTM; Duncan et al., 2007; Strahan et al., 2007, 2013). The GMI CTM is driven by meteorological fields from the Modern-Era Retrospective analysis for Research and Applications, version 2 (MERRA-2; Gelaro et al., 2017). GMI CTM simulations used in this study have 1° latitude x 1.25° longitude horizontal resolution ($\sim$ 100 km) with 72 vertical levels, extending from the surface to 0.01 hPa.

The chemical mechanism of the CTM includes tropospheric and stratospheric chemistry with approximately 120 species and over 400 reactions. In addition to the spectrum of chemical processes dependent upon the model meteorology, several aspects of O_3 production and destruction also depend on the meteorology: biogenic emissions (temperature, photosynthetically active radiation), soil emissions of NO_x (temperature, precipitation), lightning emissions of NO_x (convective mass flux), wet deposition (wind, clouds, precipitation), and dry deposition (wind, clouds, temperature, pressure). Additional information about the natural and anthropogenic emission inventories and model parameterizations (e.g., biogenic emissions, lightning NO_x, etc.) is provided in Kerr et al. (2019) and Strode et al. (2015).

The GMI CTM is a proven model to understand surface-level O_3 variability and its drivers (e.g., Duncan et al., 2008; Strode et al., 2015; Kerr et al., 2019). Kerr et al. (2019) evaluated the CTM with observations from an *in-situ* network in the U.S. and showed that the model skillfully simulated the observed daily variability of O_3 during the summer despite a high model bias in the eastern U.S. and low model bias in the western U.S; these biases are common among CTMs (e.g., Brown-Steiner et al., 2015; Guo et al., 2018; Phalitnonkiat et al., 2018).

In this study we focus on the O_3-meteorology relationships in the Northern Hemisphere for a three-year period (2008−2010) during boreal summer (1 June−31 August). We use O_3 from the model's surface level, which has a nominal thickness of $\sim$ 130 m. CTM output from the early afternoon (mean 1300 − 1400 local time), coinciding with the overpass time of the Afternoon Constellation ("A-Train") of Earth observing satellites, was archived as gridded fields, whereas hourly output was archived only at select sites. We consequently use modeled O_3 from this early afternoon period, noting that this time of day typically represents a time in which the PBL is well-mixed (e.g., Cooper et al., 2012) and daily O_3 concentrations reach their maximum (e.g., Schnell et al., 2014). Considering O_3 during this early afternoon period versus longer averaging periods leads to similar results (Kerr et al., 2019).

Two simulations are analyzed in this study. The first is a control simulation with daily (or sub-daily) variations in meteorology, chemistry, and natural emissions. Anthropogenic emissions in this simulation vary from month to month. Unless otherwise indicated, all subsequent figures and analysis use this control simulation. In a second simulation referred to as "transport-only," we isolate the role of transport. Meteorological fields related to transport such as pressure, wind, convection, PBL height, and precipitation (as it affects the vertical transport of O_3 via wet deposition) all vary on daily and sub-daily timescales in this transport-only simulation. The daily variations of other meteorological fields that affect chemistry and emissions (e.g., temperature, clouds and albedo-related variables, surface roughness, specific humidity, soil moisture, and ground wetness) are removed by using a single, monthly mean diurnal curve for each of these fields at each grid cell. Therefore, any process that relies on these variables (e.g., photolytic and kinetic reaction rates, biogenic emissions, dry deposition) is identical for a given time of the diurnal cycle for all days in a particular month. Other non-biogenic emissions are fixed to a single monthly mean value with no diurnal variations. We note that although there are no day-to-day variations in emissions- and chemistry-related processes within a given month in the transport-only simulation, there is still seasonal and interannual variability. This transport-only simulation is similar to the "Transport" simulation discussed in Kerr et al. (2019) with the exception that specific humidity is also averaged to a monthly mean diurnal cycle.

2.2 Observations

We use *in-situ* observations of O_3 across North America, Europe, and China to examine the observed variations of the O_3-meteorology relationships and assess the accuracy of the GMI CTM. We choose these regions because their *in-situ* networks, described below, measure and archive O_3 hourly. Since the model outputs O_3 averaged over 1300-1400 hours (local time), comparing this output with hourly O_3 observations averaged over the same time of the day represents the most direct comparison. The lack of *in-situ* networks with observations at a high temporal frequency in many other parts of the world hinders our ability to examine model performance over other regions.

Observations of O_3 from 233 Canadian sites are part of the National Air Pollution Surveillance Network (NAPS), collected and analyzed by Environment and Climate Change Canada (ECCC, 2017). In the U.S. we use observations from the Air Quality System (AQS), which contains O_3 observations collected by the U.S. Environmental Protection Agency and state, local, and tribal air pollution control agencies at 1483 sites (EPA, 2019). The European Monitoring and Evaluation Programme (EMEP) provides O_3 observations at 142 sites in the European Union (Hjellbrekke & Solberg, 2019).

For China we use observations from the Chinese Ministry of Ecology and Environment (MEE) for summers 2016−2017 (Li et al., 2019). Observations are primarily from urban centers, and if a particular Chinese city has > 1 monitor, a city-wide average was computed following Z. Zhao and Wang (2017), resulting in data from 360 Chinese cities. The choice of this $2016 - 2017$ time period is because this Chinese observational network did not come online until the mid-2010s. Accordingly, when we assess the performance of the GMI CTM and discuss the observed O_3-meteorology relationships in China, we use model simulations (Section 2.1) and reanalysis data (Section 2.3) for 2016−2017 rather than the $2008 - 2010$ period used elsewhere in this study.

2.3 Meteorological Reanalysis

In addition to providing meteorological input to drive the GMI CTM, MERRA-2 is also used to determine the relationships between O_3 and meteorology. Several of the observational networks detailed in Section 2.2 lack co-located meteorological observations, and Varotsos et al. (2013) commented that lack of co-located O_3 and temperature (or other meteorological) observations necessitates the use of gridded products to examine the relationships between O_3 and meteorology.

MERRA-2 meteorological fields are not available at the satellite overpass times sampled by the GMI CTM simulations (Section 2.1). We calculate daily averages from the following MERRA-2 fields: hourly surface-level (10-m) zonal (U_{10}) and meridional (V_{10}) wind, three-hourly 2-m specific humidity (q), three-hourly 500 hPa zonal wind (U_{500}), and hourly PBL height ($PBLH$). Daily 2-m maximum temperature (T) is computed as the maximum of hourly values. Our use of daily maximum temperature follows Zhang and Wang (2016) and Meehl et al. (2018).

There are uncertainties associated with an assimilated product like MERRA-2, but Bosilovich et al. (2015) presented evidence that MERRA-2 provides a very good quality reanalysis data set. As the MERRA-2 data have higher horizontal resolution than the GMI CTM (0.5° latitude × 0.625° longitude for MERRA-2 versus 1° latitude ×1.25°

longitude for the CTM), we degrade the MERRA-2 data to the resolution of the CTM using xESMF, a universal regridding tool for geospatial data (Zhuang, 2018).

2.4 Methodology

2.4.1 Statistical analysis

We use the Pearson product-moment correlation coefficient and the slope of the ordinary least squares (OLS) regression (denoted $r(x, y)$ and dy/dx for variables x and y, respectively) to (1) quantify the O_3-meteorology relationships on daily timescales and (2) evaluate the ability of the GMI CTM to accurately simulate observed O_3 from the *in-situ* networks detailed in Section 2.2. The correlation coefficient is a parametric test that measures the degree of linear correlation between x and y, and the OLS regression describes the linear relationship between x (explanatory variable) and y (dependent variable).

The serial dependence (persistence) in our meteorological and chemical data reduces the effective sample size by an amount not known *a priori* and inhibits the use of traditional hypothesis testing methods such as t-tests to evaluate significance (Zwiers & von Storch, 1995; Wilks, 1997; Mudelsee, 2003). Therefore, we use moving block bootstrapping to quantify the significance of the correlation coefficient. While traditional bootstrapping resamples individual, independent values of the time series, moving block bootstrapping resamples continuous subsets of the time series with blocklength L and does not destroy the ordering responsible for the persistence (Wilks, 2011). At each grid cell we synthetically construct a null distribution of 10000 bootstrapped realizations of the correlation coefficient (Mudelsee, 2014) and use $L = 10$ days. As a rule of thumb, blocklengths should generally exceed the decorrelation time. More rigorous methods for optimizing L exist, but we find that $L = 10$ is adequate for our application and our results are not sensitive to the exact value of L. To evaluate the significance, we estimate the 95% confidence interval using the percentile method of the bootstrapped values (i.e., the 95% confidence interval of our 10000 realizations is given by the 250th and 9750th sorted values). If this confidence interval does not contain zero, we declare the correlation coefficient significant.

2.4.2 Jet stream position

We define the latitude of the jet (ϕ_{jet}) as the latitude of maximum zonal winds at 500 hPa (U_{500}) on each day. This approach to determine ϕ_{jet} follows Barnes and Fiore (2013) but differs in two ways: (1) Barnes and Fiore (2013) determined ϕ_{jet} using U_{500} averaged over the eastern North America zonal sector. We determine ϕ_{jet} locally (at each longitudinal grid cell) and between 20−70°N; (2) After finding the maximum U_{500} for each longitude, we employ a simple moving average that is essentially a convolution of daily ϕ_{jet} of a general rectangular pulse with width $\sim 10°$. This approach removes large changes (abrupt latitudinal shifts) in ϕ_{jet} with longitude. Using smoothed versus unsmoothed data or different pulse widths yields similar overall findings in this study.

2.4.3 Cyclone detection and tracking

To assess the impact of extratropical cyclones on surface-level O_3, we use the MAP Climatology of Mid-latitude Storminess (MCMS) database to locate cyclones (Bauer & Genio, 2006; Bauer et al., 2016). Within MCMS, cyclones are detected as minima in the ERA-Interim sea level pressure (SLP) dataset (Dee et al., 2011) and are subject to additional filters to screen for spurious detections. Once detected, MCMS tracks cyclones with criteria that require gradual changes in SLP, no sudden changes in direction, and cyclones travel distances less than 720 km over single six-hourly time steps. Additional details can be found in Bauer and Genio (2006) and Bauer et al. (2016).

3 Global O_3 distribution and evaluation

We begin with an analysis of the distribution and variability of modeled surface-level O_3 during summer (Figure 1a). Concentrations of O_3 are highest ($\sim 30-60$ ppbv) in a broad mid-latitude band over continental regions extending from $20-50°$N. The GMI CTM suggests that O_3 is not zonally-symmetric within this mid-latitude band and that the highest mean concentrations (> 50 ppbv) are in the Middle East and central and eastern Asia. Outside of the mid-latitudes, the CTM simulates lower O_3 concentrations (< 30 ppbv), and the lowest concentrations in the hemisphere (< 15 ppbv) are found in the remote tropical marine atmosphere. We characterize the daily variability of O_3 by the standard deviation, and two levels (8 and 10 ppbv) are highlighted with the thin dashed and thick contours in Figure 1a. The hemispheric distribution of mean summertime surface O_3 and its variability in Figure 1a is consistent with simulations from other models in a recent model intercomparison (Turnock et al., 2020).

To illustrate the possible influence of anthropogenic emissions on the spatial variability of mean O_3 concentrations, we show mean annual anthropogenic NO_x emission data from the Emissions Database for Global Atmospheric Research (EDGAR; Crippa et al., 2018) at their native resolution (0.1° latitude x 0.1° longitude) in Figure 1b. EDGAR is used in the GMI CTM, but is overwritten by regional inventories, if available. To first order, regions with the highest O_3 concentrations and largest O_3 variability generally coincide with industrialized regions that have high precursor emissions (Figure 1).

We evaluate whether the modeled O_3 distribution shown in Figure 1a is realistic using the correlation coefficient, calculated for CTM grid cells containing *in-situ* monitors (Section 2.2). The temporal correlation between modeled and observed $O_3 > 0.5$ in the vast majority of grid cells (Figure 2). The strength of the correlation is slightly weaker in central China than other parts of China or Europe and North America (compare Figures 2c and 2a-b), but there are no other readily-detectable spatial patterns regarding the strength of the correlation.

The primary goal of our study is to document the O_3-meteorology relationships in terms of the strength of the temporal correlation of O_3 with temperature and humidity. Thus, the model's ability to accurately reproduce this covariance (Figure 4) is the relevant litmus test for model performance. Recent studies by Strode et al. (2015) and Kerr et al. (2019) have shown that the GMI CTM can reproduce the meteorological- and emissions-driven variability of summertime O_3 as well as the O_3-temperature relationship over the U.S. On account of these studies and our analysis in Figure 2, the GMI CTM is a suitable tool to address our research questions. The agreement between the observed and modeled O_3-meteorology correlations will be explored in the following section (Section 4), and this analysis will also support our use of the GMI CTM to simulate the covariance of O_3 with temperature or humidity.

4 O_3-meteorology relationships

In this section we describe the relationships among O_3, temperature, and humidity on daily timescales in the Northern Hemisphere during summer. We primarily use the GMI CTM but also compare the modeled relationships to observed values. As discussed in the Introduction (Section 1), other studies have focused mainly on subsets of the Northern Hemisphere mid-latitudes, but our examination of the relationships across the entire hemisphere allows us to have a more holistic sense of the synoptic-scale variations of these relationships.

In the mid-latitudes ($\sim 30-60°$N), statistically-significant positive values of $r(T, O_3)$ are simulated by the CTM throughout North America and Eurasia (Figure 3a), but over virtually all the oceans $r(T, O_3)$ is negative. Poleward of the mid-latitudes, the strength of $r(T, O_3)$ decreases nearly monotonically over land, reaching either weak values or significantly negative correlations (Figure 3a). The O_3-temperature relationship is varied equatorward of the mid-latitudes; but, in the zonal mean, $r(T, O_3)$ decreases to negative values south of 30°N. Previous work by Rasmussen et al. (2012) and Brown-Steiner et al. (2015) in the U.S. and Han et al. (2020) and Lu, Zhang, Chen, et al. (2019) in China showed a similar latitudinal gradient of $r(T, O_3)$. Despite the general tendency of a positive-to-negative relationship between O_3 and temperature with decreasing latitude, there are regions at low latitudes with significant positive correlations between O_3 and temperature (Central America, Sahel, the south coast of the Arabian Peninsula, Indo-Gangetic Plain; Figure 3a).

The sign of $r(q, O_3)$ generally transitions from significantly positive in the continental mid-latitudes to significantly negative over continental regions at higher and lower latitudes and over the oceans (Figure 3b). Unlike $r(T, O_3)$, the sign of $r(q, O_3)$ outside of the mid-latitudes is more spatially uniform. The only exceptions to the widespread negative correlations occur over small parts of the Mediterranean Sea and Caribbean and Indian Oceans (Figure 3b). These results are supported by modeling and observational studies in the U.S. and China, which indicate $r(q, O_3) > 0$ in the northern U.S. and China and $r(q, O_3) < 0$ in southern U.S. and China (e.g., Tawfik & Steiner, 2013; Kavassalis & Murphy, 2017; Li et al., 2019).

In continental regions of the mid-latitudes, temperature is a better predictor of O_3 than specific humidity, as $r(T, O_3) > r(q, O_3)$. Other studies support temperature as a leading covariate in the mid-latitudes (e.g., Camalier et al., 2007; Porter et al., 2015; Otero et al., 2016; Sun et al., 2017; Kerr & Waugh, 2018).

Many other studies report $\mathrm{d}O_3/\mathrm{d}T$ (Rasmussen et al., 2012; S. Zhao et al., 2013; Brown-Steiner et al., 2015; Kerr et al., 2019; Porter & Heald, 2019), and we also present $\mathrm{d}O_3/\mathrm{d}T$ and $\mathrm{d}O_3/\mathrm{d}q$ in Figure S1a-b for comparisons with these other studies. The spatial variations of the slopes shown in Figure S1a-b are qualitatively similar to $r(T, O_3)$ and $r(q, O_3)$ shown in Figure 3, as is expected by construction. We also note that the large-scale patterns in Figure 3 are preserved whether $r(T, O_3)$ and $r(q, O_3)$ or $\mathrm{d}O_3/\mathrm{d}T$ and $\mathrm{d}O_3/\mathrm{d}q$ are calculated with daily data aggregated over summers 2008−2010 or with daily data from individual summers.

To test whether the modeled O_3-meteorology relationships are realistic, we calculate $r(T, O_3)$ and $r(q, O_3)$ from the *in-situ* networks described in Section 2.2. The strength of the zonally-averaged values of observed and modeled $r(T, O_3)$ and $r(q, O_3)$ generally reaches a maximum around 50°N across four distinct regions (Figure 4). In Europe and the eastern U.S., the CTM slightly overestimates the strength of $r(T, O_3)$ and $r(q, O_3)$ by $\sim 0.1-0.3$, similar to other studies (e.g., Brown-Steiner et al., 2015; Kerr et al., 2019). Since we used temperature from MERRA-2 to calculate the observed $r(T, O_3)$ and $r(q, O_3)$ (some of the observational networks lack co-located meteorological measurements), differences in the O_3-meteorology relationships are driven by differences in simulated versus observed O_3 rather by temperature. Observations are sparse outside of the mid-latitudes. A small number of AQS monitors in Alaska and NAPS monitors in northern Canada supports the transition of $r(T, O_3)$ and $r(q, O_3)$ from positive to negative at high latitudes that is suggested by the model (Figure 4).

In summary, the observation- and model-based analysis of the relationships among surface-level O_3, temperature, and humidity reveals substantial variability across the Northern Hemisphere during summer. The terrestrial mid-latitudes ($\sim 30-60$°N) stand out as the largest, most spatially-coherent region with significant positive relationships of O_3 with temperature and humidity (Figures 3-4). The O_3-meteorology relationships are negative over nearly all marine regions, while they are mixed in sign and often not significant at high and low latitude continental regions (Figures 3-4).

5 Factors causing the O_3-meteorology relationships

The O_3-meteorology relationships in Figure 3 are far from uniform, and their spatial structure begs the question: what factors drive these relationships? In Section 1, we discussed several direct and indirect drivers that have been linked to O_3 variability, such as emissions, chemistry, and transport. Recent work has shown that transport-related processes are key contributors to the O_3-temperature relationship in the U.S. and Europe (Kerr et al., 2019; Porter & Heald, 2019), and we expand on these previous findings and examine the covariance of O_3 with temperature and humidity over the Northern Hemisphere. We do this using the transport-only GMI CTM simulation in which the daily variability of chemistry and emissions are fixed (Section 2.1).

The transport-only simulation achieves similar mean O_3 concentrations as the control simulation (compare Figures 1a and S2a). Percentage differences in mean O_3 between simulations are generally less than $\pm 5\%$, suggesting that the non-linearities underpinning O_3 chemistry do not drastically change mean O_3 concentrations when day-to-day variations in chemistry- and emissions-related processes are removed. Regions in Figure 1a with high NO_x (and presumably other precursor) emissions such as the eastern U.S., Europe, and China experience the largest decrease in mean O_3 concentrations as the daily variability of chemistry- and emissions-related processes are removed (Figure S2).

The O_3-meteorology relationships calculated with O_3 from the transport-only simulation are remarkably similar to the same quantities from the control simulation (e.g., compare Figures S1a-b and S1c-d), emphasizing the dominance of transport on these relationships. As the transport-only simulation used monthly mean values or monthly averaged diurnal cycles for processes related to chemistry and emissions, it is possible that some of the daily correlations over the three summers in our measuring period could be due to month-to-month or interannual variations in temperature or humidity coupled to chemistry or emissions. However, Porter and Heald (2019) found a similar dominance of transport in their simulations where summertime averaged values were used (rather than monthly averages). Furthermore, when we repeat the correlation analysis (i.e., Figure 3) using daily data from individual months (rather than the combined nine months) we find good agreement between the correlations from control and transport-only simulations with both showing the key features (e.g., positive correlations over mid-latitude continental regions, negative values over the oceans). Taken all together, these results indicate transport is the dominant process driving the O_3-meteorology relationships across Northern Hemisphere mid-latitudes.

Over most of the oceans and a majority of the continental regions in the Northern Hemisphere, the strength of the O_3-meteorology relationships slightly increases in the transport-only simulation (negative values in Figures 5, S1e-f). The hatching in Figures 5 and S1e-f indicates that the significance of the O_3-meteorology relationships is largely retained when only daily variations in transport-related processes are considered.

There are a few regions such as the eastern U.S. and southeast Asia where the daily variability of chemistry and emissions appears important for the O_3-meteorology relationships (Figures 5, S1e-f). In these regions the strength of the correlation and the magnitude of the slopes decreases up to $\sim 50\%$ in the transport-only simulation and the correlation coefficient switches from significant to not significant. We note that these regions have high levels of anthropogenic emissions (e.g., NO_x; Figure 1b) and biogenic emissions (e.g., isoprene; Guenther et al., 2012). Further work is warranted to understand how emissions (and the chemical processes linking emissions to O_3 production) contribute to the O_3-meteorology relationships in these regions.

Although *daily* variations in chemistry- and emissions-related processes do not drive the O_3-meteorology relationships across the Northern Hemisphere, the importance of chemistry and emissions in setting the background state should not be ignored. To illustrate this, we return to Figure 3 and draw attention to the stark land-ocean contrasts in the O_3-meteorology relationships with marine regions generally characterized by negative correlations. These marine regions are largely low NO_x environments (Figure 1a). In this type of chemical regime, an increase in humidity or temperature is expected either to not impact or decrease O_3 (e.g., Johnson et al., 1999; Coates et al., 2016). The transport-only simulation still includes this low NO_x marine environment relative to other regions, just without day-to-day variations.

These results answer our original question whether daily variations in transport, chemistry, or emissions are primarily responsible for the O_3-meteorology relationships, but they also raise the question of which aspect(s) of transport links temperature and humidity to O_3. In the next section we investigate the role of the jet stream on surface-level temperature, humidity, and O_3, and we also develop and test hypotheses to link synoptic-scale flow aloft to meteorology and composition at the surface.

5.1 The role of the jet stream

Barnes and Fiore (2013) determined that the largest O_3 variability and peak strength of $r(T, O_3)$ are located near ϕ_{jet} in the eastern U.S. These results were further explored by Shen et al. (2015) who found that O_3 responded to seasonal variations in the position of the jet stream and that a poleward shift of the jet increased O_3 concentrations south of the jet. In this section we expand upon this previous work and document the response of surface-level O_3, temperature, and humidity to daily changes in ϕ_{jet} across the Northern Hemisphere.

The time-averaged latitude of the jet stream ($\overline{\phi_{jet}}$) is shown by the scatter points in Figure 1, and $\overline{\phi_{jet}}$ averaged over the entire hemisphere is 50.1°N. The variability of the jet, cast in terms of the standard deviation, averaged over the Northern Hemisphere is 10.5°, but its variability is not constant throughout the hemisphere (vertical bars in Figure 1). Rather, we note the largest variability over continental regions, particularly Eurasia ($\sim 20°$), and smaller variability over maritime regions, coinciding with the Atlantic and Pacific storm tracks. The position of the jet is only one metric to describe the jet stream, and other jet-related measures exist (e.g., strength of the jet, waviness). Our focus on ϕ_{jet} rather than other metrics is based on Ordóñez et al. (2019) who found that ϕ_{jet} exerts a stronger influence than the strength of the jet on surface-level pollution extremes.

The maximum variability of O_3 (Figure 1a) and the strength of the O_3-meteorology correlations (Figures 3-5) peak at or slightly south of ϕ_{jet}, and ϕ_{jet} also separates regions with elevated O_3 concentrations to its south from regions with low (< 30 ppbv) concentrations to its north (Figure 1a). These results are consistent with Barnes and Fiore (2013); however, it is worth pointing out a couple of exceptions: (1) In Asia, O_3 variability peaks over a broader latitudinal range, extending from ϕ_{jet} to $\sim 20°$N (Figure 1). (2) There are regions with significant positive values of $r(T, O_3)$ such as the Sahel and India that do not coincide with ϕ_{jet} (Figure 3a). Our current work also reveals the weak-to-negative correlation between O_3 and humidity or temperature for marine environments and some high and low latitudes.

To further examine the role of the jet stream on the O_3-meteorology relationships, we segregate summer days into two subsets: days when the jet stream is in poleward (PW) and equatorward (EW) position. Days classified as PW (EW) are days in which ϕ_{jet} exceeds (is less than) the 70th (30th) percentile of all daily ϕ_{jet} at each longitudinal grid cell. We construct composites of O_3, temperature, and humidity by identifying the average value of these fields on days with a PW or EW jet stream and thereafter calculate the difference of these PW and EW composites.

The difference in the PW and EW composites (PW - EW) of O_3, temperature, and humidity are positive in the mid-latitudes over land (Figure 6), which indicates that these fields increase when the jet is in a more northerly position. The positive values are generally significant (hatching in Figure 6), coincide with the latitudinal band over which the jet stream migrates, and persist $10 - 15°$ north and south of $\overline{\phi_{jet}}$ over land. Outside the continental mid-latitudes, the association between the position of the jet and O_3, temperature, or humidity is weak and not statistically significant (Figure 6).

In contrast, there is a difference in the response of O_3 to the jet stream versus temperature and humidity over the mid-latitude ocean basins. In the case of O_3, a poleward movement of the jet decreases O_3 over the oceans but increases it over land, while temperature increases over both land and oceans (Figure 6a). This sharp land-ocean contrast, akin to the land-ocean contrasts in the O_3-meteorology correlations (Figure 3), could reflect land-ocean asymmetries in O_3 and its precursors and will be further explored in Section 5.3. On the other hand, temperature and humidity increase over the oceans as the jet shifts poleward, akin to the behavior of these variables over land (Figure 6b-c). The impact of the jet stream on O_3, temperature, and humidity outside of the mid-latitudes is largely not significant (Figure 6).

For completeness, maps of the correlation of jet distance with the variables in Figure 6 are shown in Figure S3. We note that the strength of the correlation between ϕ_{jet} and O_3 and meteorology is weaker than $r(T, O_3)$ and $r(q, O_3)$, and the spatial extent of areas with significant correlations is smaller (compare Figures 3 and S3).

While the response of O_3 and meteorological fields to the meridional movement of the jet stream is consistent in its sign in the mid-latitudes over land, there are some regions outside of the continental mid-latitudes where jet movement leads to increases of one variable and decreases of another. China is an example of this. As the jet migrates poleward, O_3 significantly increases, as it does throughout the mid-latitudes; however, temperature remains more or less constant, and humidity slightly decreases (Figures 6, S3). This discrepancy and others evident in Figures 6 and S3, particularly those at lower latitudes and over the oceans, are beyond the scope of this study, but future studies should further examine and address regions where O_3, temperature, and humidity are decoupled from the jet in this manner.

Having uncovered the dominant role of transport and the connections with the jet, we next explore transport-related processes that might be responsible for the relationships among surface-level O_3, the jet stream, and meteorology. As cyclones are commonly-invoked to explain O_3 variability, we begin by showing the impact of the jet stream on cyclone frequency and, in turn, the effect of cyclones on O_3. We then explore and discuss how the jet stream affects the surface-level meridional flow and commensurate changes in O_3, temperature, and humidity.

5.2 Cyclones

Mid-latitude baroclinic cyclones follow a storm track dictated by the jet stream, and changes in ϕ_{jet} affect the location of this storm track (e.g., Shen et al., 2015). To assess the dependence of cyclone frequency on ϕ_{jet}, we show the spatial distribution of the climatological frequency of cyclones detected by MCMS (Section 2.4.3) in Figure 7a. The highest frequency of mid-latitude cyclone detections largely follows ϕ_{jet} and is offset north of the jet by $\sim 10°$ over North America. In other regions such as eastern Asia the peak cyclone frequency occurs in a broader latitudinal band, extending north and south of ϕ_{jet} by $\sim 15°$ (Figure 7a).

We identify the subset of days with a poleward-shifted or equatorward-shifted jet using the 70th and 30th percentiles of the daily latitudes of the jet stream, as previously described, to determine the dependence of cyclones on ϕ_{jet}. We thereafter determine the frequency of cyclones on these subsets of days and show the difference (Figure 7b). The meridional movement of the jet affects cyclones in two different ways. First, the total number of cyclones on days when the jet is in a poleward position is 15% less than on days when the jet is equatorward. Second, the storm track shifts alongside the jet, and cyclones are more highly concentrated about ϕ_{jet} when the jet is equatorward compared with when it is poleward (Figure 7b).

The decrease and latitudinal shift in cyclone frequency with meridional movements of the jet stream could be the transport-related mechanism responsible for the above O_3-meteorology relationships. The cold fronts associated with mid-latitude cyclones have been suggested as a mechanism for the ventilation of the eastern U.S. (Mickley, 2004), and Knowland et al. (2015) and Jaeglé et al. (2017) demonstrated how cyclones redistribute O_3, its precursors, and other pollutants vertically and horizontally in the atmosphere. We assess the impact of cyclones on surface-level O_3 by further filtering the cyclones from the MCMS dataset (Section 2.4.3), requiring that a particular cyclone (1) occurs over land and (2) is detected for ≥ 2 six-hourly time steps to allow us to calculate the direction of propagation. We then rotate cyclones following Knowland et al. (2015) and Knowland et al. (2017) such that they propagate to the right of Figure 8 to account for the impact of different ascending and descending airstreams within the cyclones. Applying these filters to cyclones in summers $2008 - 2010$ yields ~ 730 cyclones with an average lifetime of ~ 54 hours. The mean direction of cyclone propagation is east-southeast ($\sim 120°$, where $0°$ is north). Though we have only considered cyclones occurring over land in this analysis, compositing all land- and ocean-based cyclones produces O_3 anomalies of similar magnitude.

The largest negative O_3 anomaly occurs in the "cold sector" of the cyclone, and the largest positive anomaly occurs in the "warm sector," However, these positive and negative anomalies cancel each other when averaged over the footprint of the cyclones, leading to a net $\sim$ 0 ppbv change in O_3 (Figure 8). Comparing our results with conceptual models and case studies of baroclinic cyclones (e.g., Cooper et al., 2004; Polvani & Esler, 2007) hints that the positive anomalies in Figure 8 occur near the warm conveyor belt (WCB), where there is likely polluted air entrained from the PBL and lower troposphere. On the other hand, the largest negative anomalies are found in the vicinity of the dry intrusion (DI) and could be influenced by cleaner air entrained from the upper troposphere or lower stratosphere. The roles of the WCB in ventilating pollution *from* the PBL and the cleaner air brought *to* the PBL by the DI could cancel each other out and be one reason for the small increases and decreases in surface-level O_3.

If cyclones were the mechanism that linked ϕ_{jet} to surface-level O_3, we might expect that the cyclones-driven impact on O_3 would be > 6 ppbv in the mid-latitudes, similar to the impact that ϕ_{jet} has on O_3 (Figure 6a). However, our analysis in Figure 8 indicates that, on average, cyclones have a much weaker effect on surface-level O_3, despite the connections between cyclones and the jet stream (Figure 7b). There is, though, substantial variability among individual cyclones (the standard deviation of the O_3 anomaly is a factor of ~ 6 greater than the largest anomaly; Figure 8). As such, some cyclones might be effective at reducing surface-level O_3, but this is far from the case for all cyclones.

Other studies support the small role of cyclones on surface-level O_3. Knowland et al. (2015) showed that the surface-level O_3 anomaly associated with springtime cyclones in the North Atlantic and Pacific is small (i.e., $-5 < \delta\, O_3 < 5$ ppbv); however, they found a larger impact when examining the mid- to upper-level O_3 anomalies. Moreover, Leibensperger et al. (2008) found a negative correlation between the number of O_3 pollution events and the number of mid-latitude cyclones passing through the southern climatological storm track ($\sim 40{-}50°$N) over eastern North America on interannual timescales, but Turner et al. (2012) demonstrated that the cyclone-O_3 correlation is weak, and cyclone frequency explains less than 10% of the variability of O_3 pollution events in the region.

In summary, while the storm track dictating the preferred location of baroclinic cyclones shifts with the jet (Figure 7b), cyclones are likely not the key mechanism controlling O_3 variability in the Northern Hemisphere mid-latitudes as they only explain a small fraction of the changes of O_3 associated with daily migrations of the jet (Figure 8).

5.3 Meridional transport

The ventilation and dilution of the PBL, the surface-level zonal flow (U_{10}), or the total wind ($\overline{U_{10}}$) could link the position of the jet stream to surface-level O_3. However, an analysis of $PBLH$, U_{10}, and $\overline{U_{10}}$ rules out these variables as drivers of the O_3-jet relationship (Text S1-S2, Figures S4-5). To summarize: ϕ_{jet} is not significantly correlated with variations in $PBLH$ and $\overline{U_{10}}$ throughout the majority of the Northern Hemisphere. Similar to our analysis of cyclones in Figures 7-8, U_{10} is significantly correlated with ϕ_{jet} throughout parts of the mid-latitudes but not correlated with O_3 independently of the jet.

However, the surface-level meridional flow (V_{10}) is significantly correlated with the position of the jet in the mid-latitudes (Figure 9a). When the jet is in a poleward position, V_{10} increases by more than 2 m/s throughout the mid-latitudes with the largest increases centered over the oceans (Figure 9a). In the mid-latitudes, time-averaged V_{10} is varied in sign but generally weak ($-0.5 < V_{10} < 0.5$), so the large values of V_{10} accompanying a poleward jet represent a large increase in the southerly flow.

In addition to its connections with ϕ_{jet}, V_{10} is significantly positively correlated with O_3 in the continental mid-latitudes (Figure 9b). Here, the strength of $r(V_{10}, O_3)$ rivals that of $r(T, O_3)$ and $r(q, O_3)$ (compare Figures 9b and 3), suggesting that the surface-level meridional flow is also a key covariate of O_3 variability on daily timescales. In parts of the mid-latitudes such as eastern North America or Asia, a unit increase in V_{10} is associated with an increase of O_3 that is roughly one-third of its total daily variability (Figure S6). Equatorward of the mid-latitudes (particularly for $\sim 10-30°$N), V_{10} is significantly negatively correlated with O_3, while $r(V_{10}, O_3)$ is not significant poleward of the mid-latitudes. Thus far we have shown significant positive relationships among ϕ_{jet}, V_{10}, O_3, and the meteorological variables in the mid-latitudes (Figures 6a, 9). When the jet is poleward, surface-level meridional flow becomes strongly southerly, and there is significant poleward advection of O_3, temperature, and humidity.

We posit that the relationships of O_3 with ϕ_{jet} and the meteorological variables are largely the product of surface-level meridional flow acting on the latitudinal background gradients. Ozone generally peaks south of ϕ_{jet} (Figure 1a), so there are negative gradients in the vicinity of the jet (Figure 9b). These negative gradients are well-aligned with the regions where there is increased southerly flow at the surface when the jet is poleward (Figure 9a). This configuration serves to advect higher concentrations of O_3 into the mid-latitudes when the jet is poleward (Figures 9b, S6). Although not shown here, the latitudinal gradients of temperature and humidity are broadly similar to $dO_3/d\phi$ inasmuch as they are positive south of the mid-latitudes. When surface-level southerly flow increases, these gradients favor increases of temperature and humidity in the mid-latitudes, as is evident in Figure 6b-c.

The importance of the background gradient can also partially explain the negative O_3-jet relationships over the oceans. Latitudes where $dO_3/d\phi > 0$ often extend farther poleward over the oceans than over land. For example, over the Pacific storm track $dO_3/d\phi > 0$, while $dO_3/d\phi < 0$ between ~ 20 and 40°N in the Pacific (Figure 9b). Under these conditions, increased southerly flow associated with the poleward movement of the jet would decrease O_3 (i.e., a negative O_3-jet relationship). Other factors also may be important in marine environments. For example, strong surface-level zonal winds in the vicinity of the Atlantic and Pacific storm tracks may lead to zonal gradients that are as important as the meridional background gradients investigated in this section.

The importance of both meridional flow and the latitudinal background gradient has been the subject of recent studies for O_3 and other trace gases. Keppel-Aleks et al. (2012) showed that the daily variability of total column carbon dioxide was dominated by non-local effects and primarily reflects the synoptic scale latitudinal carbon dioxide gradient. Changes in the mean meridional circulation (specifically the extratropical stratospheric-to-tropospheric transport associated with the Southern Hemisphere Hadley Cell) have been suggested to explain recent trends in Southern Hemisphere tropospheric O_3 (Lu, Zhang, Zhao, et al., 2019). On smaller spatial scales, transport-related features favoring southerly flow (e.g., the nocturnal low-level jet in the U.S.) are important for explaining O_3 in the PBL (Taubman et al., 2004). Our future work will further elucidate the main physical features that link the jet stream, surface-level meridional flow, and background tracer gradients.

In the mid-latitudes, the meridional vacillation of the jet stream impacts the surface-level meridional flow (Figure 9a). The meridional flow, in turn, plays a profound role in surface-level O_3 variability (Figure 9b). Temperature, humidity, and O_3 are generally higher south of ϕ_{jet}, and the meridional flow acts on their background gradients and leads to the coupling between the jet stream and O_3 and the meteorological variables shown in Figure 6.

6 Conclusions

The primary intent of this study was to document the relationships among surface-level O_3, temperature, and humidity and explore the cause(s) of these relationships. Both observations and the GMI CTM support substantial spatial variations in $r(T, O_3)$ and $r(q, O_3)$. In continental regions of the mid-latitudes ($\sim 30-60°$N), the O_3-meteorology relationships are significantly positive (Figures 3-4). The O_3-meteorology relationships are significantly negative over the oceans (Figure 3). For other continental regions outside the mid-latitudes, $r(T, O_3)$ and $r(q, O_3)$ are generally weak and often not statistically significant, but we have shown regions at low latitudes (e.g., Central America, Sahel) that are exceptions to this rule-of-thumb (Figure 3).

Our transport-only GMI CTM simulation indicates that the O_3-temperature and O_3-humidity relationships are largely driven by transport-related phenomena on daily timescales (Figure 5). We stress that these findings do not trivialize the importance of chemistry and emissions. Chemistry- and emissions-related processes are essential for setting the background state for the production of a secondary pollutant such as O_3; however, daily variations in these processes are not the dominant drivers of O_3 variability or its covariance with temperature and humidity. Our results showcasing the dominant role of transport are in line with previous work by Kerr et al. (2019) and Porter and Heald (2019), which showed that a majority of the O_3-temperature relationship in the U.S. and Europe derive from meteorological phenomena.

The variability of surface-level O_3, temperature, and humidity are linked to the meridional movement of the jet stream in the Northern Hemisphere mid-latitudes. This result extends previous work focusing on the eastern U.S. (e.g., Barnes & Fiore, 2013; Shen et al., 2015) to the entire Northern Hemisphere. Over land in the mid-latitudes, a poleward (equatorward) shift of the jet is associated with increased (decreased) surface-level O_3, temperature, and humidity (Figures 6, S3). Over the oceans, temperature and humidity respond to this meridional vacillation of the jet in the same fashion as over land, but the poleward (equatorward) movement of the jet decreases (increases) O_3.

We ultimately found that the jet influences these surface-level fields by means of changes in the surface-level meridional flow. On days when the jet is in a poleward position, the pronounced southerly flow in the mid-latitudes together with the latitudinal gradients of O_3, temperature, and humidity generally lead to increases of O_3, temperature, and humidity in the mid-latitudes (Figures 6, 9). We have shown clear land-ocean differences in the relationships among O_3, temperature or specific humidity, and the jet stream (Figures 3, 6, S3). We partially attribute these the land-ocean contrasts to differences in the latitudinal gradient of O_3 over land versus over the ocean (Figure 9b).

Establishing the spatial variations of the O_3-meteorology relationships is a prerequisite to understand which regions could experience an "O_3-climate penalty" (Wu et al., 2008) under future climatic changes. As the O_3-meteorology relationships in the present-day climate are far from uniform in both magnitude and sign, it is unlikely that future changes in the climate will affect O_3 uniformly. Furthermore, as the relationships among O_3, temperature, and humidity are driven by an indirect association with transport, caution should be used when applying any measures of the current sensitivity of O_3 to meteorological variables (e.g., dO_3/dT or dO_3/dq from Figure S1) to future climatic changes.

Overall, our results demonstrate the importance of the position of the jet stream and surface-level meridional flow on O_3 variability in the Northern Hemisphere, both of which will be affected by the future climate (e.g., Barnes & Polvani, 2013; Shaw & Voigt, 2015; Grise et al., 2019). A robust poleward displacement of the jet stream is expected in the twenty-first century, while changes to other properties of the jet (i.e., variations in speed; north-south movement) will exhibit spatial heterogeneity (Barnes & Polvani, 2013). The effect of these changes on surface-level O_3 needs to be explored.

Acknowledgments

G. H. Kerr is supported by the NSF IGERT Program (Grant No. 1069213). The authors would like to thank Dr. Emma Knowland for her thoughtful comments to improve the manuscript. The MERRA-2 data used in this study have been provided by the Global Modeling and Assimilation Office (GMAO) at NASA Goddard Space Flight Center. The data may be obtained at `gmao.gsfc.nasa.gov/reanalysis/MERRA-2/`. NASA GMI CTM output is publicly available on the data portal for the NASA Center for Climate Simulation (`portal.nccs.nasa.gov/datashare/dirac`). The control simulation can be found at the following path: `/gmidata2/users/mrdamon/Hindcast-Family/HindcastMR2/`. Hourly observations of O_3 are available for (1) China at `beijingair.sinaapp.com`, (2) the European Union at `projects.nilu.no//ccc/emepdata.html`, (3) Canada at `maps-cartes.ec.gc.ca/rnspa-naps/data.aspx`, and (4) the U.S. at `aqs.epa.gov/aqsweb/airdata/download_files.html`. MCMS development is supported by NASA's Earth Science Program for Modeling, Analysis, and Prediction (MAP), and data can be found at `gcss-dime.giss.nasa.gov/mcms/`.

References

Barnes, E. A., & Fiore, A. M. (2013). Surface ozone variability and the jet position: Implications for projecting future air quality. *Geophys. Res. Lett.*, *40*(11), 2839–2844. doi: 10.1002/grl.50411

Barnes, E. A., & Polvani, L. (2013). Response of the midlatitude jets, and of their variability, to increased greenhouse gases in the CMIP5 models. *J. Clim.*, *26*(18), 7117–7135. doi: 10.1175/JCLI-D-12-00536.1

Barrett, B. S., Raga, G. B., Retama, A., & Leonard, C. (2019). A multiscale analysis of the tropospheric and stratospheric mechanisms leading to the March 2016 extreme surface ozone event in Mexico City. *J. Geophys. Res.*, *124*(8), 4782–4799. doi: 10.1029/2018JD029918

Bauer, M., & Genio, A. D. D. (2006). Composite analysis of winter cyclones in a GCM: Influence on climatological humidity. *J. Clim.*, *19*(9), 1652–1672. doi: 10.1175/jcli3690.1

Bauer, M., Tselioudis, G., & Rossow, W. B. (2016). A new climatology for investigating storm influences in and on the extratropics. *J. Appl. Meteorol. Climatol.*, *55*(5), 1287–1303. doi: 10.1175/jamc-d-15-0245.1

Bosilovich, M., Akella, S., Coy, L., Cullather, R., Draper, C., Gelaro, R., et al. (2015). *MERRA-2: Initial evaluation of the climate, NASA/TM–2015-104606* (Vol. 43).

Brown-Steiner, B., Hess, P., & Lin, M. (2015). On the capabilities and limitations of GCCM simulations of summertime regional air quality: A diagnostic analysis of ozone and temperature simulations in the US using CESM CAM-Chem. *Atmos. Environ.*, *101*, 134–148. doi: 10.1016/j.atmosenv.2014.11.001

Camalier, L., Cox, W., & Dolwick, P. (2007). The effects of meteorology on ozone in urban areas and their use in assessing ozone trends. *Atmos. Environ.*, *41*(33), 7127–7137. doi: 10.1016/j.atmosenv.2007.04.061

Coates, J., Mar, K. A., Ojha, N., & Butler, T. M. (2016). The influence of temperature on ozone production under varying NO_x conditions – a modelling study. *Atmos. Chem.Phys.*, *16*(18), 11601–11615. doi: 10.5194/acp-16-11601-2016

Cooper, O. R., Forster, C., Parrish, D., Trainer, M., Dunlea, E., Ryerson, T., et al. (2004). A case study of transpacific warm conveyor belt transport: Influence of merging airstreams on trace gas import to North America. *J. Geophys. Res. Atmos.*, *109*(D23). doi: 10.1029/2003jd003624

Cooper, O. R., Gao, R.-S., Tarasick, D., Leblanc, T., & Sweeney, C. (2012). Long-term ozone trends at rural ozone monitoring sites across the United States, 1990–2010. *J. Geophys. Res.*, *117*, D22307. doi: 10.1029/2012JD018261

Crippa, M., Guizzardi, D., Muntean, M., Schaaf, E., Dentener, F., van Aardenne, J. A., et al. (2018). Gridded emissions of air pollutants for the period 1970–2012 within EDGAR v4.3.2. *Earth Syst. Sci. Data*, *10*(4), 1987–2013. doi: 10.5194/essd-10-1987-2018

Dawson, J. P., Adams, P. J., & Pandis, S. N. (2007). Sensitivity of ozone to summertime climate in the eastern USA: A modeling case study. *Atmos. Environ.*, *41*(7), 1494–1511. doi: 10.1016/j.atmosenv.2006.10.033

Dee, D. P., Uppala, S. M., Simmons, A. J., Berrisford, P., Poli, P., Kobayashi, S., et al. (2011). The ERA-Interim reanalysis: Configuration and performance of the data assimilation system. *Q. J. R. Meteorol. Soc.*, *137*(656), 553–597. doi: 10.1002/qj.828

Derwent, R. G., Witham, C. S., Utembe, S. R., Jenkin, M. E., & Passant, N. R. (2010). Ozone in central England: The impact of 20 years of precursor emission controls in Europe. *Environ. Sci. Policy*, *13*(3), 195–204. doi: 10.1016/j.envsci.2010.02.001

Duncan, B. N., Strahan, S. E., Yoshida, Y., Steenrod, S. D., & Livesey, N. (2007). Model study of the cross-tropopause transport of biomass burning pollution. *Atmos. Chem. Phys.*, *7*(14), 3713–3736.

Duncan, B. N., West, J. J., Yoshida, Y., Fiore, A. M., & Ziemke, J. R. (2008). The influence of European pollution on ozone in the Near East and northern Africa. *Atmos. Chem. Phys.*, *8*(8), 2267–2283. doi: 10.5194/acp-8-2267-2008

ECCC. (2017). *National air pollution surveillance program.* `https://open.canada.ca/data/en/dataset/1b36a356-defd-4813-acea-47bc3abd859b`. (Retrieved on 22 July 2019)

EPA. (2019). *Air quality system data mart.* `http://www.epa.gov/ttn/airs/aqsdatamart`. (Retrieved on 23 July 2019)

Fiore, A. M., Naik, V., & Leibensperger, E. M. (2015). Air quality and climate connections. *J. Air Waste Manage.*, *65*(6), 645–685. doi: 10.1080/10962247.2015.1040526

Gelaro, R., McCarty, W., Suárez, M. J., Todling, R., Molod, A., Takacs, L., et al. (2017). The Modern-Era Retrospective Analysis for Research and Applications, Version 2 (MERRA-2). *J. Clim.*, *30*(14), 5419–5454. doi: 10.1175/JCLI-D-16-0758.1

Grise, K. M., Davis, S. M., Simpson, I. R., Waugh, D. W., Fu, Q., Allen, R. J., et al. (2019). Recent tropical expansion: Natural variability or forced response? *J. Clim.*, *32*(5), 1551–1571. doi: 10.1175/jcli-d-18-0444.1

Guenther, A. B., Jiang, X., Heald, C. L., Sakulyanontvittaya, T., Duhl, T., Emmons, L. K., & Wang, X. (2012). The Model of Emissions of Gases and Aerosols from Nature version 2.1 (MEGAN2.1): An extended and updated framework for modeling biogenic emissions. *Geosci. Mod. Dev.*, *5*(6), 1471–1492. doi: 10.5194/gmd-5-1471-2012

Guo, J. J., Fiore, A. M., Murray, L. T., Jaffe, D. A., Schnell, J. L., Moore, C. T., & Milly, G. P. (2018). Average versus high surface ozone levels over the continental USA: Model bias, background influences, and interannual variability. *Atmos. Chem. Phys.*, *18*(16), 12123–12140. doi: 10.5194/acp-18-12123-2018

Han, H., Liu, J., Shu, L., Wang, T., & Yuan, H. (2020). Local and synoptic meteorological influences on daily variability of summertime surface ozone in eastern China. *Atmos. Chem. Phys.*, 203–222. doi: 10.5194/acp-20-203-2020

He, H., Stehr, J. W., Hains, J. C., Krask, D. J., Doddridge, B. G., Vinnikov, K. Y., et al. (2013). Trends in emissions and concentrations of air pollutants in the lower troposphere in the Baltimore/Washington airshed from 1997 to 2011. *Atmos. Chem. Phys.*, *13*(15), 7859–7874. doi: 10.5194/acp-13-7859-2013

Hegarty, J., Mao, H., & Talbot, R. (2007). Synoptic controls on summertime surface ozone in the northeastern United States. *J. Geophys. Res.*, *112*(D14). doi: 10.1029/2006JD008170

Hjellbrekke, A.-G., & Solberg, S. (2019). *Ozone measurements 2017* (EMEP/CCC-Report No. 2/2019). Kjeller, Norway: EMEP Co-operative Programme for Monitoring and Evaluation of the Long-range Transmission of Air Pollutants in Europe. Retrieved from `https://projects.nilu.no//ccc/reports/cccr2-2019_Ozone.pdf`

Jacob, D. J., & Winner, D. A. (2009). Effect of climate change on air quality. *Atmos. Environ.*, *43*(1), 51–63. doi: 10.1016/j.atmosenv.2008.09.051

Jaeglé, L., Wood, R., & Wargan, K. (2017). Multiyear composite view of ozone enhancements and stratosphere-to-troposphere transport in dry intrusions of Northern Hemisphere extratropical cyclones. *J. Geophys. Res.*, *122*(24), 13,436–13,457. doi: 10.1002/2017jd027656

Johnson, C. E., Collins, W. J., Stevenson, D. S., & Derwent, R. G. (1999). Relative roles of climate and emissions changes on future tropospheric oxidant concentrations. *J. Geophys. Res. Atmos.*, *104*(D15), 18631–18645. doi: 10.1029/1999jd900204

Kavassalis, S. C., & Murphy, J. G. (2017). Understanding ozone-meteorology correlations: A role for dry deposition. *Geophys. Res. Lett.*, *44*(6), 2922–2931. doi: 10.1002/2016GL071791

Keppel-Aleks, G., Wennberg, P. O., Washenfelder, R. A., Wunch, D., Schneider, T., Toon, G. C., et al. (2012). The imprint of surface fluxes and transport on variations in total column carbon dioxide. *Biogeosciences*, *9*(3), 875–891. doi: 10.5194/bg-9-875-2012

Kerr, G. H., & Waugh, D. W. (2018). Connections between summer air pollution and stagnation. *Environ. Res. Lett.*, *13*(8), 084001. doi: 10.1088/1748-9326/aad2e2

Kerr, G. H., Waugh, D. W., Strode, S. A., Steenrod, S. D., Oman, L. D., & Strahan, S. E. (2019). Disentangling the drivers of the summertime ozone-temperature relationship over the United States. *J. Geophys. Res.*, *124*(19), 10503–10524. doi: 10.1029/2019jd030572

Kim, S.-W., Heckel, A., McKeen, S. A., Frost, G. J., Hsie, E.-Y., Trainer, M. K., et al. (2006). Satellite-observed U.S. power plant NO_x emission reductions and their impact on air quality. *Geophys. Res. Lett.*, *33*(22). doi: 10.1029/2006GL027749

Knowland, K. E., Doherty, R. M., & Hodges, K. I. (2015). The effects of springtime mid-latitude storms on trace gas composition determined from the MACC reanalysis. *Atmos. Chem. Phys.*, *15*(6), 3605–3628. doi: 10.5194/acp-15-3605-2015

Knowland, K. E., Doherty, R. M., Hodges, K. I., & Ott, L. E. (2017). The influence of mid-latitude cyclones on European background surface ozone. *Atmos. Chem. Phys.*, *17*(20), 12421–12447. doi: 10.5194/acp-17-12421-2017

Landrigan, P. J., Fuller, R., Acosta, N. J. R., Adeyi, O., Arnold, R., Basu, N., et al. (2018). The lancet commission on pollution and health. *Lancet*, *391*(10119), 462–512. doi: 10.1016/s0140-6736(17)32345-0

Lefohn, A. S., Malley, C. S., Smith, L., Wells, B., Hazucha, M., Simon, H., et al. (2018). Tropospheric ozone assessment report: Global ozone metrics for climate change, human health, and crop/ecosystem research. *Elem. Sci. Anth.*, *6*(1), 28. doi: 10.1525/elementa.279

Leibensperger, E. M., Mickley, L. J., & Jacob, D. J. (2008). Sensitivity of US air quality to mid-latitude cyclone frequency and implications of 1980–2006 climate change. *Atmos. Chem. Phys.*, *8*(23), 7075–7086.

Li, K., Jacob, D. J., Liao, H., Shen, L., Zhang, Q., & Bates, K. H. (2019). Anthropogenic drivers of 2013–2017 trends in summer surface ozone in China. *Proc. Natl. Acad. Sci. U.S.A.*, *116*(2), 422–427. doi: 10.1073/pnas.1812168116

Lin, M., Horowitz, L. W., Payton, R., Fiore, A. M., & Tonnesen, G. (2017). US surface ozone trends and extremes from 1980 to 2014: Quantifying the roles of rising Asian emissions, domestic controls, wildfires, and climate. *Atmos. Chem. Phys.*, *17*(4), 2943–2970. doi: 10.5194/acp-17-2943-2017

Lu, X., Zhang, L., Chen, Y., Zhou, M., Zheng, B., Li, K., … Zhang, Q. (2019). Exploring 2016–2017 surface ozone pollution over China: Source contributions and meteorological influences. *Atmos. Chem. Phys.*, *19*(12), 8339–8361. doi: 10.5194/acp-19-8339-2019

Lu, X., Zhang, L., Zhao, Y., Jacob, D. J., Hu, Y., Hu, L., et al. (2019). Surface and tropospheric ozone trends in the Southern Hemisphere since 1990: Possible linkages to poleward expansion of the Hadley circulation. *Sci. Bull.*, *64*(6), 400–409. doi: 10.1016/j.scib.2018.12.021

Meehl, G. A., Tebaldi, C., Tilmes, S., Lamarque, J.-F., Bates, S., Pendergrass, A., & Lombardozzi, D. (2018). Future heat waves and surface ozone. *Environ. Res. Lett.*, *13*(6), 064004. doi: 10.1088/1748-9326/aabcdc

Mickley, L. J. (2004). Effects of future climate change on regional air pollution episodes in the United States. *Geophys. Res. Lett.*, *31*(24). doi: 10.1029/2004GL021216

Mudelsee, M. (2003). Estimating Pearson's correlation coefficient with bootstrap confidence interval from serially dependent time series. *Math. Geol.*, *35*(6), 651–665. doi: 10.1023/b:matg.0000002982.52104.02

Mudelsee, M. (2014). *Climate time series analysis: Classical statistical and bootstrap methods* (2nd ed.). Cham, Heidelberg, New York, Dordrecht, London: Springer International Publishing. doi: 10.1007/978-3-319-04450-7

Ordóñez, C., Barriopedro, D., & García-Herrera, R. (2019). Role of the position of the North Atlantic jet in the variability and odds of extreme PM_{10} in Europe. *Atmos. Environ.*, *210*, 35–46. doi: 10.1016/j.atmosenv.2019.04.045

Otero, N., Sillmann, J., Schnell, J. L., Rust, H. W., & Butler, T. (2016). Synoptic and meteorological drivers of extreme ozone concentrations over Europe. *Environ. Res. Lett.*, *11*(2), 024005. doi: 10.1088/1748-9326/11/2/024005

Parrish, D. D., Law, K. S., Staehelin, J., Derwent, R., Cooper, O. R., Tanimoto, H., et al. (2012). Long-term changes in lower tropospheric baseline ozone concentrations at northern mid-latitudes. *Atmos. Chem. Phys.*, *12*(23), 11485–11504. doi: 10.5194/acp-12-11485-2012

Phalitnonkiat, P., Hess, P. G. M., Grigoriu, M. D., Samorodnitsky, G., Sun, W., Beaudry, E., et al. (2018). Extremal dependence between temperature and ozone over the continental US. *Atmos. Chem. Phys.*, *18*(16), 11927–11948. doi: 10.5194/acp-18-11927-2018

Polvani, L. M., & Esler, J. G. (2007). Transport and mixing of chemical air masses in idealized baroclinic life cycles. *J. Geophys. Res.*, *112*(D23), D23102. doi: 10.1029/2007JD008555

Porter, W. C., & Heald, C. L. (2019). The mechanisms and meteorological drivers of the ozone-temperature relationship. *Atmos. Chem. Phys.*, 13367–13381. doi: 10.5194/acp-2019-140

Porter, W. C., Heald, C. L., Cooley, D., & Russell, B. (2015). Investigating the observed sensitivities of air-quality extremes to meteorological drivers via quantile regression. *Atmos. Chem. Phys.*, *15*(18), 10349–10366.

Pusede, S. E., Steiner, A. L., & Cohen, R. C. (2015). Temperature and recent trends in the chemistry of continental surface ozone. *Chem. Rev.*, *115*(10), 3898–3918. doi: 10.1021/cr5006815

Rasmussen, D. J., Fiore, A., Naik, V., Horowitz, L., McGinnis, S., & Schultz, M. (2012). Surface ozone-temperature relationships in the eastern US: A monthly climatology for evaluating chemistry-climate models. *Atmos. Environ.*, *47*, 142–153. doi: 10.1016/j.atmosenv.2011.11.021

Rasmussen, D. J., Hu, J., Mahmud, A., & Kleeman, M. J. (2013). The ozone–climate penalty: Past, present, and future. *Environ. Sci. Technol.*, *47*(24), 14258–14266. doi: 10.1021/es403446m

Reddy, P. J., & Pfister, G. G. (2016). Meteorological factors contributing to the interannual variability of midsummer surface ozone in Colorado, Utah, and other western U.S. states. *J. Geophys. Res.*, *121*(5), 2434–2456. doi: 10.1002/2015JD023840

Schnell, J. L., Holmes, C. D., Jangam, A., & Prather, M. J. (2014). Skill in forecasting extreme ozone pollution episodes with a global atmospheric chemistry model. *Atmos. Chem. Phys.*, *14*(15), 7721–7739. doi: 10.5194/acp-14-7721-2014

Shaw, T. A., & Voigt, A. (2015). Tug of war on summertime circulation between radiative forcing and sea surface warming. *Nature Geosci.*, *8*(7), 560–566. doi: 10.1038/ngeo2449

Shen, L., Mickley, L. J., & Tai, A. P. K. (2015). Influence of synoptic patterns on surface ozone variability over the eastern United States from 1980 to 2012. *Atmos. Chem. Phys.*, *15*(19), 10925–10938. doi: 10.5194/acp-15-10925-2015

Simon, H., Reff, A., Wells, B., Xing, J., & Frank, N. (2015). Ozone trends across the United States over a period of decreasing NOx and VOC emissions. *Environ. Sci. Technol.*, *49*(1), 186–195. doi: 10.1021/es504514z

Strahan, S. E., Douglass, A. R., & Newman, P. A. (2013). The contributions of chemistry and transport to low arctic ozone in March 2011 derived from aura MLS observations. *J. Geophys. Res.*, *118*(3), 1563–1576. doi: 10.1002/jgrd.50181

Strahan, S. E., Duncan, B. N., & Hoor, P. (2007). Observationally derived transport diagnostics for the lowermost stratosphere and their application to the GMI chemistry and transport model. *Atmos. Chem. Phys.*, *7*(9), 2435–2445.

Strode, S. A., Rodriguez, J. M., Logan, J. A., Cooper, O. R., Witte, J. C., Lamsal, L. N., et al. (2015). Trends and variability in surface ozone over the United States. *J. Geophys. Res.*, *120*(17), 9020–9042. doi: 10.1002/2014JD022784

Sun, W., Hess, P., & Liu, C. (2017). The impact of meteorological persistence on the distribution and extremes of ozone. *Geophys. Res. Lett.*, *44*, 1545–1553. doi:

10.1002/2016GL071731

Tai, A. P., & Martin, M. V. (2017). Impacts of ozone air pollution and temperature extremes on crop yields: Spatial variability, adaptation and implications for future food security. *Atmos. Environ.*, *169*, 11–21. doi: 10.1016/j.atmosenv.2017.09.002

Tai, A. P., Mickley, L. J., & Jacob, D. J. (2010). Correlations between fine particulate matter ($PM_{2.5}$) and meteorological variables in the United States: Implications for the sensitivity of $PM_{2.5}$ to climate change. *Atmos. Environ.*, *44*(32), 3976–3984. doi: 10.1016/j.atmosenv.2010.06.060

Taubman, B. F., Marufu, L. T., Piety, C. A., Doddridge, B. G., Stehr, J. W., & Dickerson, R. R. (2004). Airborne characterization of the chemical, optical, and meteorological properties, and origins of a combined ozone-haze episode over the Eastern United States. *J. Atmos. Sci.*, *61*(14), 1781–1793. doi: 10.1175/1520-0469(2004)061⟨1781:acotco⟩2.0.co;2

Tawfik, A. B., & Steiner, A. L. (2013). A proposed physical mechanism for ozone-meteorology correlations using land–atmosphere coupling regimes. *Atmos. Environ.*, *72*, 50–59. doi: 10.1016/j.atmosenv.2013.03.002

Turner, A. J., Fiore, A. M., Horowitz, L. W., Naik, V., & Bauer, M. (2012). Summertime cyclones over the Great Lakes storm track from 1860–2100: Variability, trends, and association with ozone pollution. *Atmos. Chem. Phys.*, *12*(8), 21679–21712. doi: 10.5194/acpd-12-21679-2012

Turnock, S. T., Allen, R. J., Andrews, M., Bauer, S. E., Emmons, L., Good, P., et al. (2020). Historical and future changes in air pollutants from CMIP6 models. *Atmos. Chem. Phys.*. doi: 10.5194/acp-2019-1211

Varotsos, K. V., Tombrou, M., & Giannakopoulos, C. (2013). Statistical estimations of the number of future ozone exceedances due to climate change in Europe. *J. Geophys. Res.*, *118*(12), 6080–6099. doi: 10.1002/jgrd.50451

Wilks, D. S. (1997). Resampling hypothesis tests for autocorrelated fields. *J. Clim.*, *10*(1), 65–82. doi: 10.1175/1520-0442(1997)010⟨0065:rhtfaf⟩2.0.co;2

Wilks, D. S. (2011). *Statistical methods in the atmospheric sciences.* Amsterdam; Boston: Elsevier Academic Press.

Woollings, T., Hannachi, A., & Hoskins, B. (2010). Variability of the North Atlantic eddy-driven jet stream. *Q. J. R. Meteorol. Soc.*, *136*(649), 856–868. doi: 10.1002/qj.625

Wu, S., Mickley, L. J., Leibensperger, E. M., Jacob, D. J., Rind, D., & Streets, D. G. (2008). Effects of 2000–2050 global change on ozone air quality in the United States. *J. Geophys. Res.*, *113*(D6). doi: 10.1029/2007JD008917

Zhang, Y., & Wang, Y. (2016). Climate-driven ground-level ozone extreme in the fall over the southeast United States. *Proc. Natl. Acad. Sci. U.S.A.*, *113*(36), 10025–10030. doi: 10.1073/pnas.1602563113

Zhao, S., Pappin, A. J., Morteza Mesbah, S., Joyce Zhang, J. Y., MacDonald, N. L., & Hakami, A. (2013). Adjoint estimation of ozone climate penalties. *Geophys. Res. Lett.*, *40*(20), 5559–5563. doi: 10.1002/2013GL057623

Zhao, Z., & Wang, Y. (2017). Influence of the West Pacific subtropical high on surface ozone daily variability in summertime over eastern China. *Atmos. Environ.*, *170*, 197–204. doi: 10.1016/j.atmosenv.2017.09.024

Zhu, J., & Liang, X.-Z. (2013). Impacts of the Bermuda High on regional climate and ozone over the United States. *J. Clim.*, *26*(3), 1018–1032. doi: 10.1175/jcli-d-12-00168.1

Zhuang, J. (2018). *Jiaweizhuang/xesmf: v0.1.1.* Zenodo. doi: https://doi.org/10.5281/ZENODO.1134366

Zwiers, F. W., & von Storch, H. (1995). Taking serial correlation into account in tests of the mean. *J. Clim.*, *8*(2), 336–351. doi: 10.1175/1520-0442(1995)008⟨0336:tsciai⟩2.0.co;2

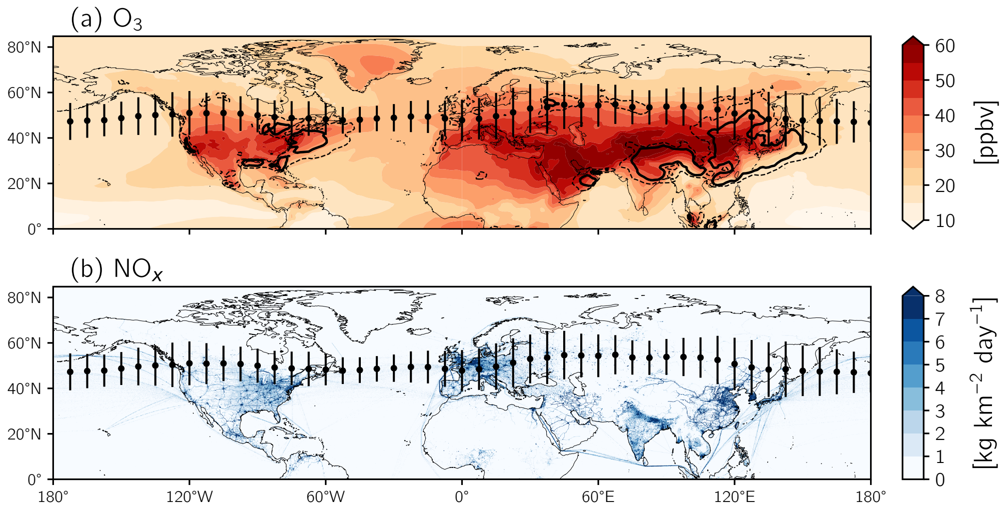

Figure 1. (a) Time-averaged O_3 from the surface-level of the GMI CTM (colored shading). Black contours indicate O_3 variability (standard deviation): thin dashed contour, 8 ppbv; thick contour, 10 ppbv. (b) Time-averaged anthropogenic NO_x emissions from EDGAR. Scatter points and vertical bars in (a-b) specify the mean position and variability of the jet stream, respectively.

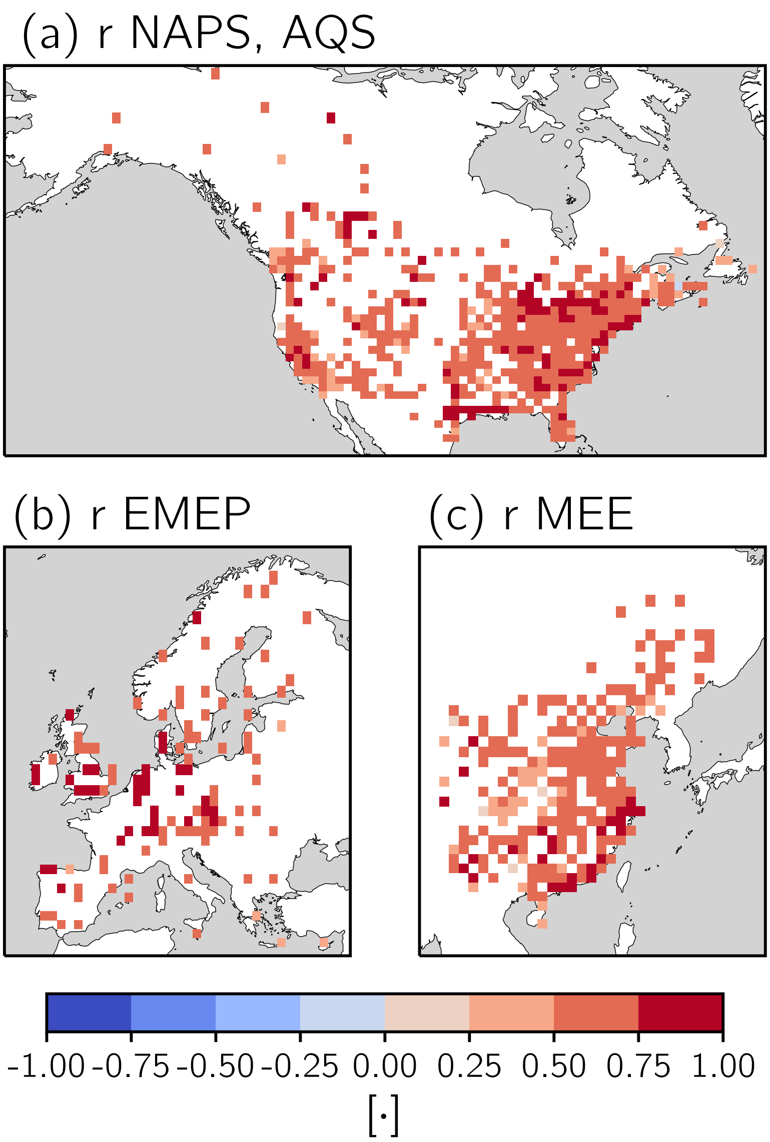

Figure 2. The correlation coefficient calculated between daily modeled O_3 from the GMI CTM and observed O_3 for model grid cells containing *in-situ* monitor(s). If there is $>$ 1 monitor in a grid cell, all O_3 observations are averaged to produce a grid cell average prior to computing the correlation coefficient. The networks in (a) North America, (b) Europe, and (c) China from which monitor-based observations have been derived are indicted in the subplots' titles. Note that the time period for the model-observation comparison in (a-b) is 2008 – 2010 but is 2016 – 2017 in (c), due to limited observations in China during earlier years.

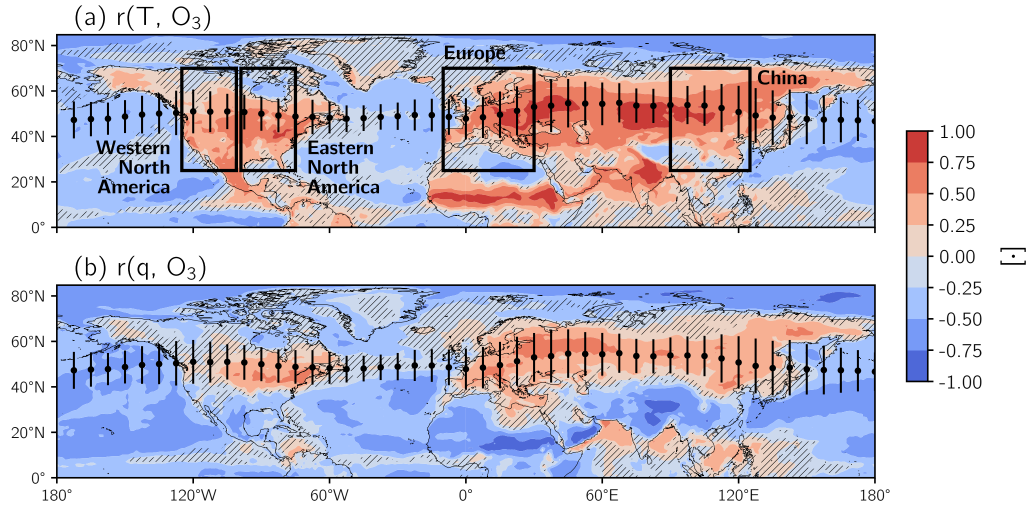

Figure 3. (a) The correlation coefficient calculated between O_3 from the GMI CTM and MERRA-2 temperature, $r(T, O_3)$. Hatching denotes regions where the correlation is not statistically significant, determined using moving block bootstrap resampling to estimate the 95% confidence interval. (b) Same as (a) but for the correlation coefficient calculated between between O_3 and MERRA-2 specific humidity, $r(q, O_3)$. Scatter points and vertical bars in (a-b) specify the mean position and variability of the jet stream, respectively. Black boxes in (a) outline the regions over which zonal averages were performed in Figure 4.

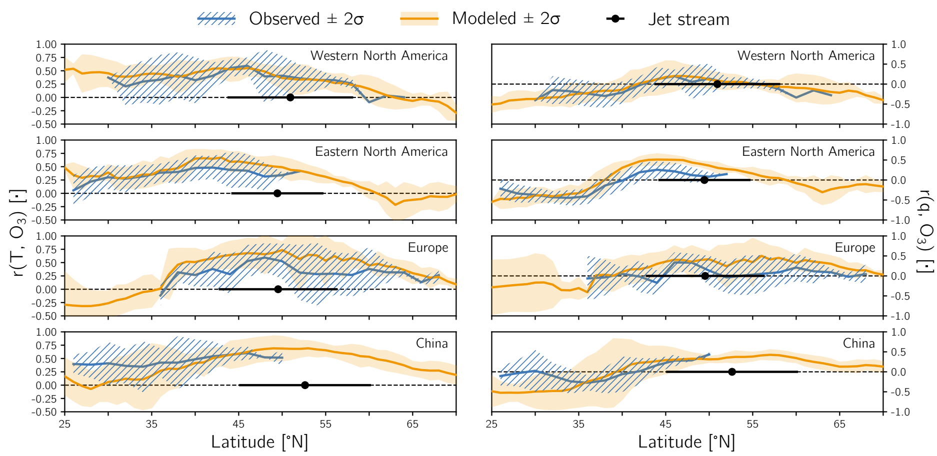

Figure 4. Zonally-averaged observed and modeled (left) $r(T, O_3)$ and (right) $r(q, O_3)$ in four regions: western North America (125° − 100°W), eastern North America (100° − 65°W), Europe (10°W−30°E), and East Asia (90 − 125°E). These regions are also outlined in Figure 3a. Zonally-averaged modeled relationships consider only grid cells over land, and the observed relationships are binned by latitude to compute the zonal average. The dashed grey lines delineate positive from negative values of the O_3-meteorology relationships, and the scatter points and vertical bars corresponding to the jet and its variability are the same as in Figure 1 but averaged over each region.

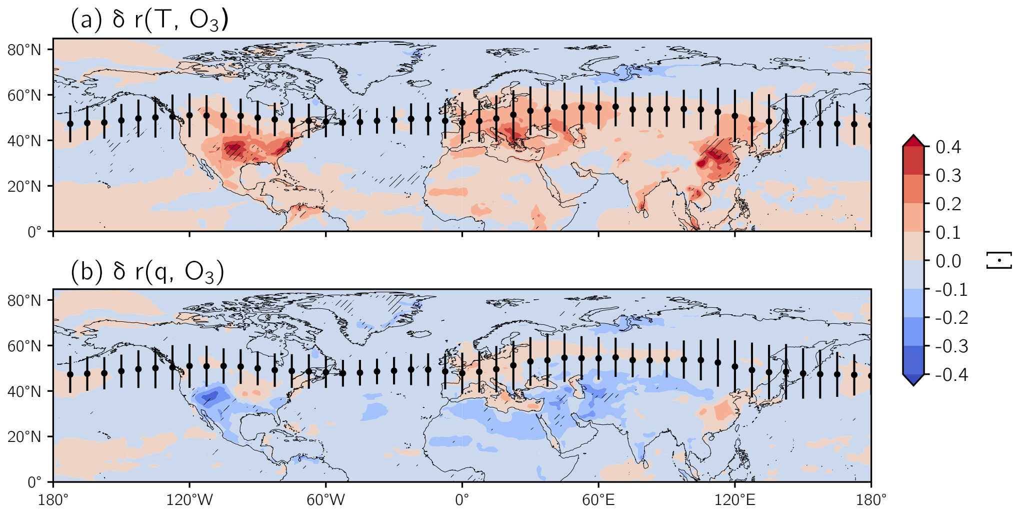

Figure 5. Differences in (a) $r(T, \mathrm{O}_3)$ and (b) $r(q, \mathrm{O}_3)$ calculated between the control and transport-only CTM simulations (i.e., control − transport-only). To assess their relative importance, differences should be compared with values from the control simulation (Figure 3). Hatching indicates regions with significant $r(T, \mathrm{O}_3)$ or $r(q, \mathrm{O}_3)$ in the control simulation that are not statistically significant in the transport-only simulation. Scatter points and vertical bars in (a-b) specify the mean position and variability of the jet stream, respectively.

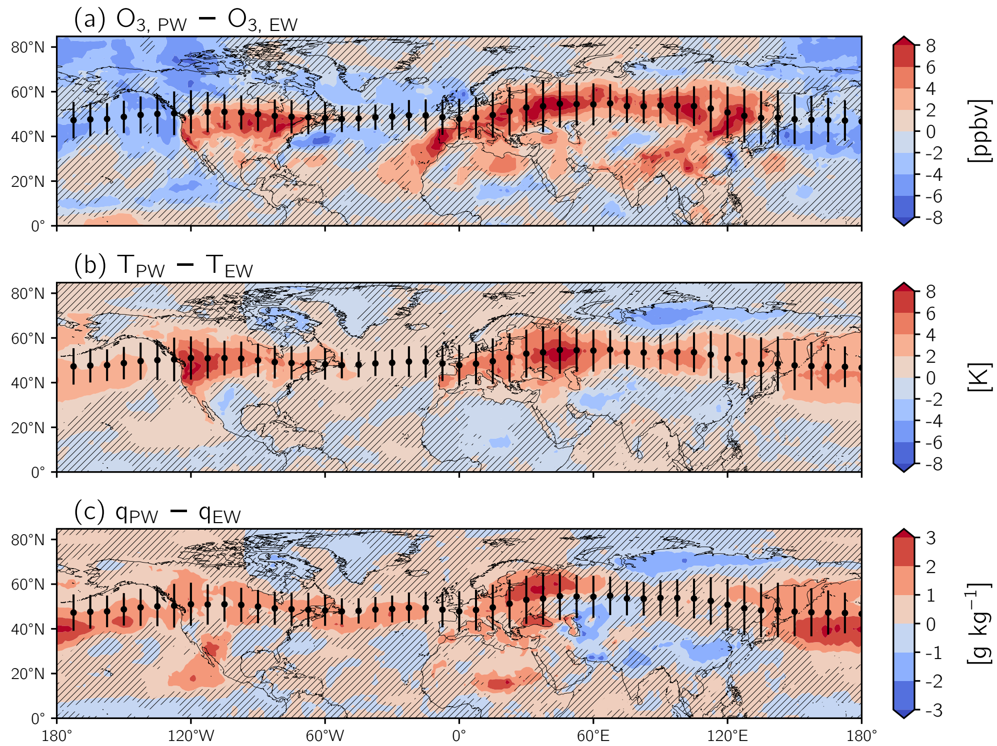

Figure 6. The difference in composites of (a) O_3, (b) temperature, and (c) specific humidity on days when the jet is in a poleward (PW) and equatorward (EW) position. Composites are formed for the PW (EW) case by determining the value of each field in (a-c) averaged over all days when the position of the jet stream (ϕ_{jet}) exceeds the 70th (is less than the 30th) percentile for each longitude. Hatching indicates regions where the correlation between each field and the distance from the jet is not statistically significant. The distance from the jet, $\phi_{jet} - \phi$, is defined as the difference, in degrees, between the latitude of the jet and the local latitude. Scatter points and vertical bars in (a-c) specify the mean position and variability of the jet stream, respectively.

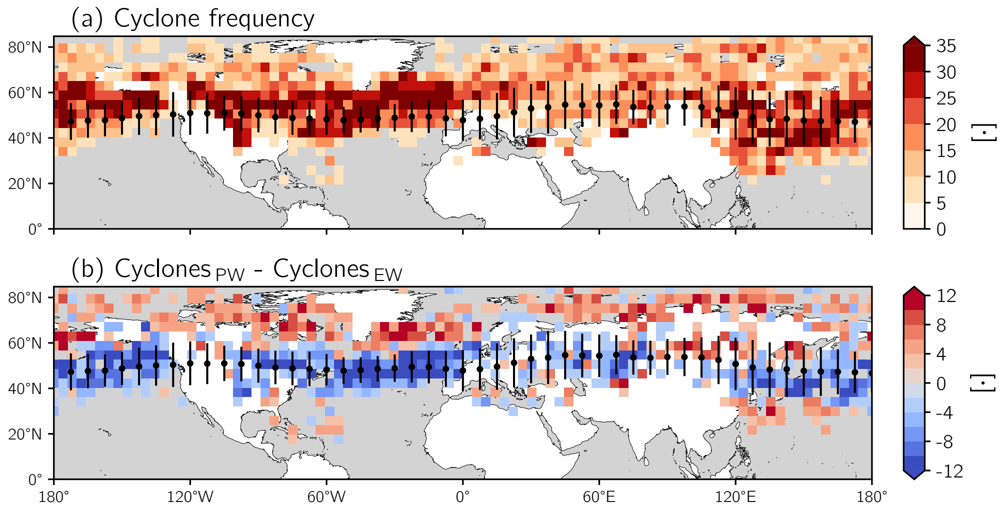

Figure 7. (a) Total number of cyclones detected by MCMS on sub-daily (six-hourly) time scales binned to a ∼ 4° × 4° grid. (b) The difference in the total number of cyclones calculated between days when the jet is in a poleward (PW) and equatorward (EW) position. Scatter points and vertical bars in (a-b) specify the mean position and variability of the jet stream, respectively.

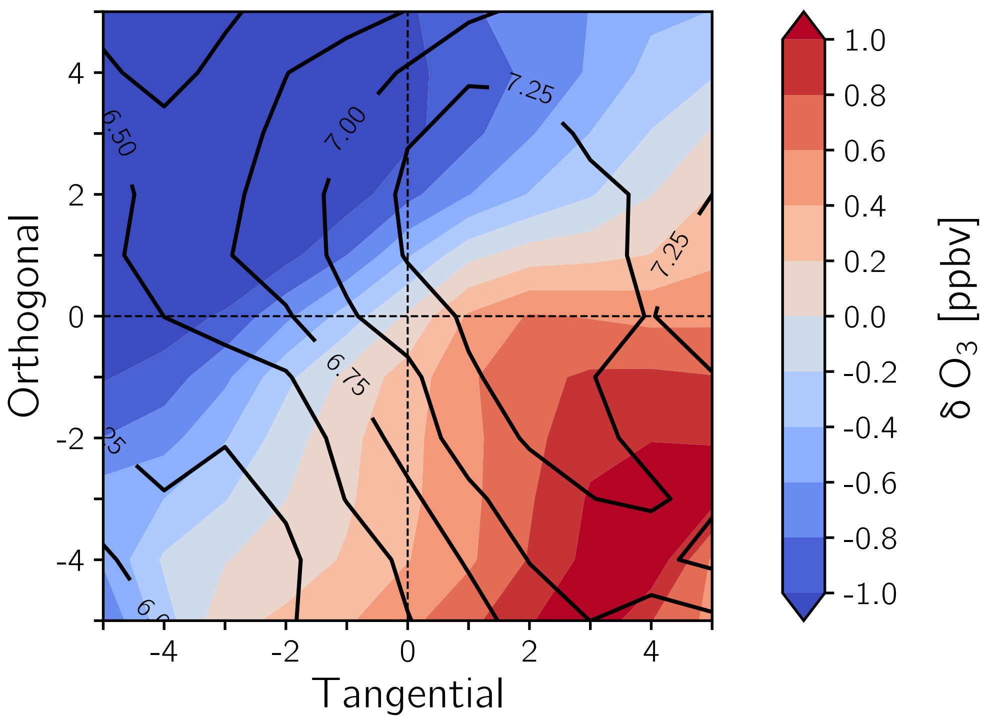

Figure 8. The average O_3 anomaly (colored shading) and standard deviation of the anomalies (solid black contours) within five grid cells ($\sim$ 5°) of the position of the cyclones. From the cyclones shown in Figure 7, we only consider cyclones occurring over land and detected for $\geq$ 2 time steps and subsequently rotate the cyclones following the direction of their propogation such that they move to the right of the figure. Dashed black lines divide the cyclone composites into quadrants.

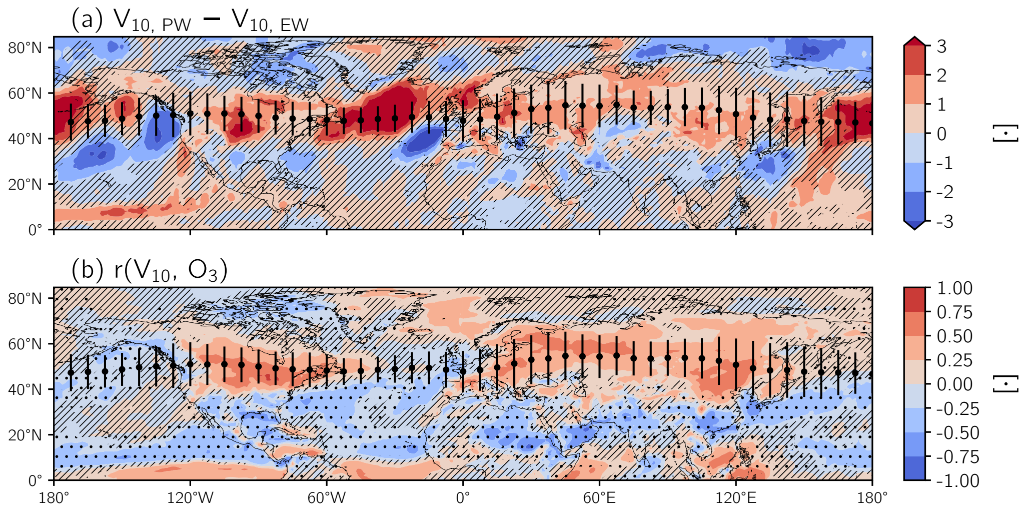

Figure 9. (a) The difference in composites of V_{10} on days when the jet is in a PW and EW position. (b) The correlation coefficient calculated between O_3 and V_{10} (colored shading) and regions where latitudinal gradient of O_3 ($dO_3/d\phi$) is positive (stippling). Scatter points and vertical bars in (a-b) specify the mean position and variability of the jet stream, respectively. Hatching denotes regions where the correlation between V_{10} and (a) the distance from jet and (b) O_3 are not statistically significant.

Supporting Information for "Surface ozone-meteorology relationships: Spatial variations and the role of the jet stream"

Gaige Hunter Kerr[1] *, Darryn W. Waugh[2,3], Stephen D. Steenrod[3,4], Sarah A. Strode[3,4], and Susan E. Strahan[3,4]

[1]Department of Earth and Planetary Sciences, Johns Hopkins University, Baltimore, Maryland, USA

[2]School of Mathematics and Statistics, University of New South Wales, Sydney, New South Wales, Australia

[3]NASA Goddard Space Flight Center, Greenbelt, Maryland, USA

[4]Universities Space Research Association, GESTAR, Columbia, Maryland, USA

Contents of this file

1. Text S1 to S2
2. Figures S1 to S6

*now at Department of Environmental and Occupational Health, George Washington University, Washington, DC, USA

Text S1: Planetary boundary layer (PBL) dynamics

Variations in the height of the PBL ($PBLH$) could connect the jet to surface-level O_3, temperature, and humidity. $PBLH$ determines vertical mixing and the dilution of surface-level pollutants (Dawson et al., 2007) and responds directly to the flux of heat into the PBL. Previous studies have used both $PBLH$ and mixing height to assess the impact of PBL dynamics on surface-level pollutants (e.g., Jacob & Winner, 2009; Reddy & Pfister, 2016), and here we use daily mean MERRA-2 $PBLH$, detailed in Section 2.3 of the main text.

An analysis of the (PW - EW) $PBLH$ composites shows that the daily north-south movement of the jet stream is not significantly associated with $PBLH$ variability over a majority of the continental regions of the Northern Hemisphere (Figures S4a, S5a). Over the oceans, northward movement of the jet stream tends to be associated with a more shallow boundary layer; but, in general, there is a no consistent sign associated with the variability of the jet with $PBLH$ (Figures S4a, S5a). This result is robust whether daily mean $PBLH$ is used as we have here, or if the jet-$PBLH$ relationship is derived using $PBLH$ averaged over subsets of the day (e.g., daytime, afternoon).

Although there is no jet-$PBLH$ relationship, it is possible that $PBLH$ may influence O_3 independently of the jet stream. To examine this we evaluate the correlation between $PBLH$ and O_3. The sign of this correlation is varied, and its strength is largely not statistically significant across the mid-latitudes (not shown). There are some regions where $r(PBLH, \mathrm{O}_3)$ is positive and significant, but this implies that a deeper PBL results in higher O_3, which goes against simple dilution arguments. These findings agree with other studies: Jacob and Winner (2009) pointed out that the effect of mixing depth on O_3 is weak or variable (while the effect of mixing depth on $PM_{2.5}$ is consistently negative).

Text S2: Near-surface zonal and total wind

Another possible mechanism for the jet-O_3 relationship is changes in surface-level flow. We form additional (PW - EW) composites and correlations for surface-level eastward (U_{10}) and total ($\overline{U_{10}}$) winds (Figures S4b-c, S5b-c).

The composites in Figure S4b-c are less meaningful unless placed in the context of the time-averaged direction and magnitude of U_{10} and $\overline{U_{10}}$. Time-averaged U_{10} is generally positive (eastward) over both land and ocean in the mid-latitudes ($40 - 60°$N) with a magnitude of ~ 1 m/s. On the other hand, $\overline{U_{10}}$ has a magnitude of < 4 m/s over land and ~ 6 m/s over the oceans.

In a $\sim 20°$ latitudinal band north of the mean position of the jet, the poleward movement of the jet significantly increases U_{10} by up to 4 m/s (Figures S4b, S5b). It is worth noting the largest areal extent of changes (both increases and decreases) in U_{10} is centered over the oceans (Figure S4b). However, U_{10} and O_3 are not correlated with each other (not shown), which rules out the surface-level zonal wind as the mechanism connecting the position of the jet stream with O_3.

We investigated the relationship between ϕ_{jet} and $\overline{U_{10}}$, a proxy for stagnation (Figures S4c and S5c). Differences in $\overline{U_{10}}$ between days with a poleward- versus equatorward-shifted jet were weak and variable in sign, and the correlation was not statistically significant across virtually the entire hemisphere. As we did with $PBLH$ and U_{10}, we considered the impact that $\overline{U_{10}}$ has on O_3 independently of the jet, as weak flow can inhibit the ventilation of the PBL (Mickley, 2004). We found that O_3 and $\overline{U_{10}}$ were generally anticorrelated in the mid-latitudes (not shown); however, these correlations were weak and not significant. There were also parts of the mid-latitudes with positive correlations between O_3 and $\overline{U_{10}}$, implying that higher wind speeds and therefore increased ventilation are associated with higher concentrations of O_3.

References

Dawson, J. P., Adams, P. J., & Pandis, S. N. (2007). Sensitivity of ozone to summertime climate in the eastern USA: A modeling case study. *Atmos. Environ.*, *41*(7), 1494–1511. doi: 10.1016/j.atmosenv.2006.10.033

Jacob, D. J., & Winner, D. A. (2009). Effect of climate change on air quality. *Atmos. Environ.*, *43*(1), 51–63. doi: 10.1016/j.atmosenv.2008.09.051

Mickley, L. J. (2004). Effects of future climate change on regional air pollution episodes in the United States. *Geophys. Res. Lett.*, *31*(24). doi: 10.1029/2004GL021216

Reddy, P. J., & Pfister, G. G. (2016). Meteorological factors contributing to the interannual variability of midsummer surface ozone in Colorado, Utah, and other western U.S. states. *J. Geophys. Res.*, *121*(5), 2434–2456. doi: 10.1002/2015JD023840

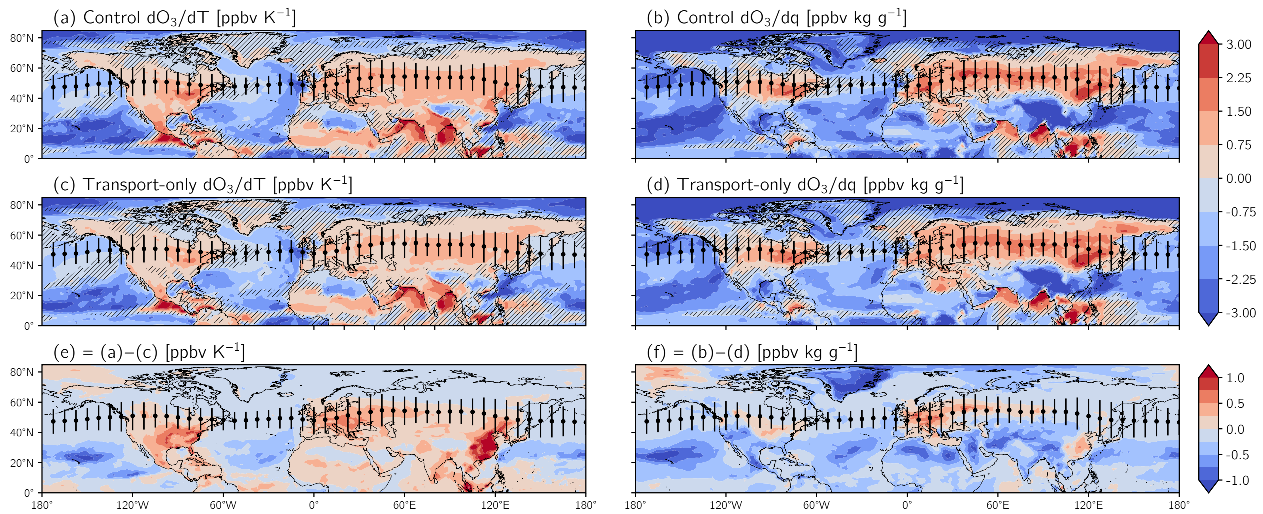

Figure S1. (a) The slope of the ordinary least squares (OLS) regression of O_3 from the control simulation versus temperature, dO_3/dT. Hatching denotes regions where the correlation between O_3 and temperature is not statistically significant. (b) Same as (a) but for O_3 from the control simulation versus humidity, dO_3/dq, with hatching showing correlations between O_3 and humidity that are not statistically significant. (c-d) Same as (a-b) but with O_3 from the transport-only simulation. (e-f) The difference in dO_3/dT and dO_3/dq between the two simulations. Scatter points and vertical bars in (a-f) specify the mean position and variability of the jet stream, respectively.

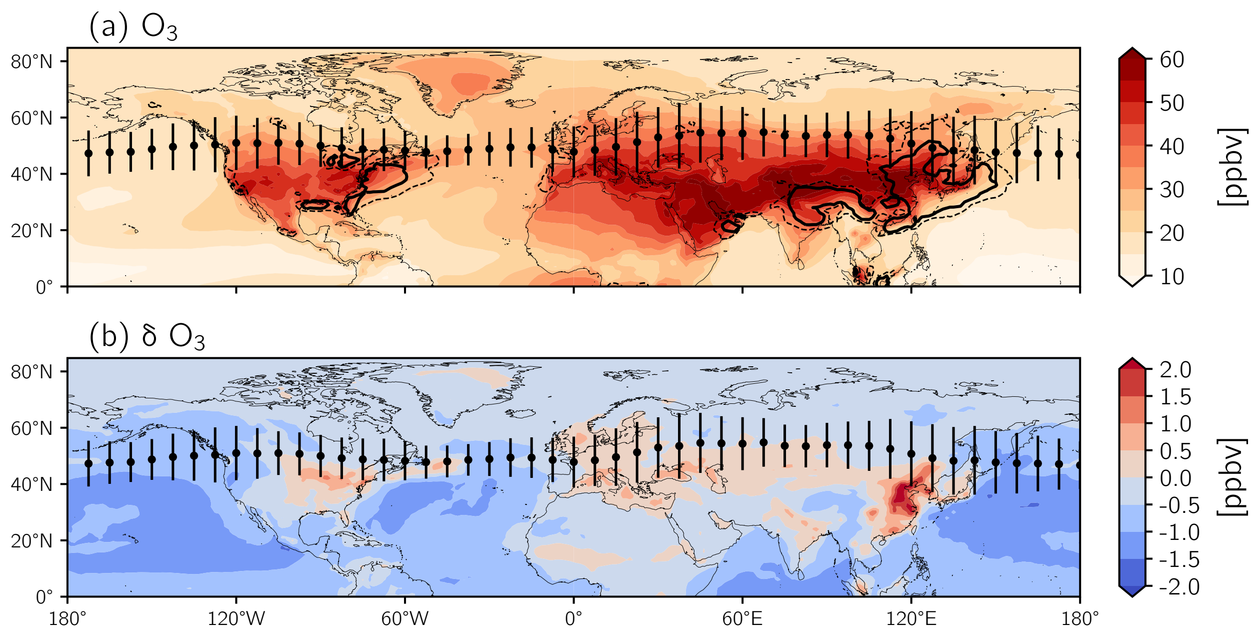

Figure S2. (a) Same as Figure 1a in the main text but for O_3 from the transport-only simulation. (b) The difference (i.e., control − transport-only) in mean O_3 concentrations. Scatter points and vertical bars in (a-b) specify the mean position and variability of the jet stream, respectively.

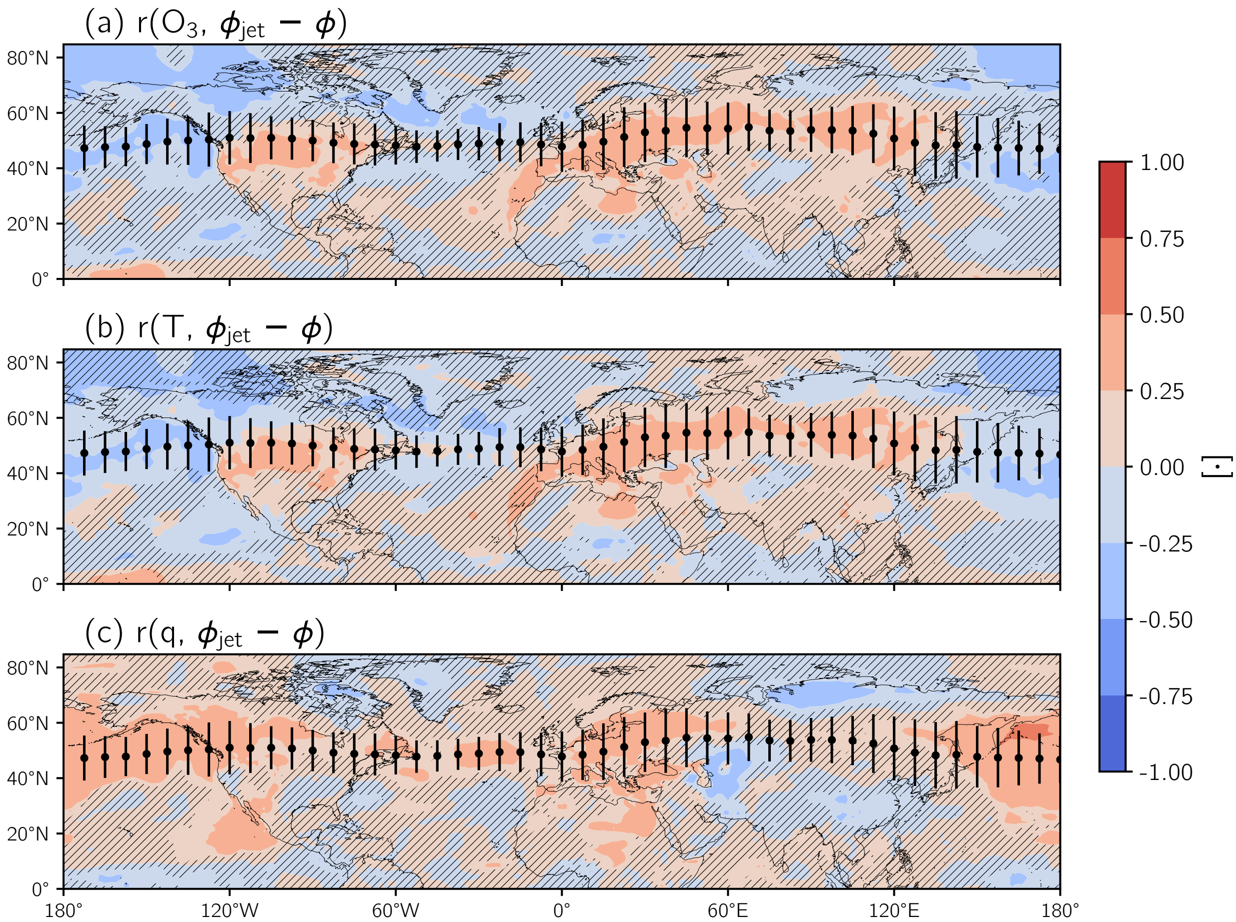

Figure S3. Colored shading shows the correlation coefficient calculated between distance from the jet stream and (a) O_3, (b) temperature, and (c) humidity. Hatching is the same as in Figure 6, and scatterpoints, and vertical bars are the same as in Figure 3.

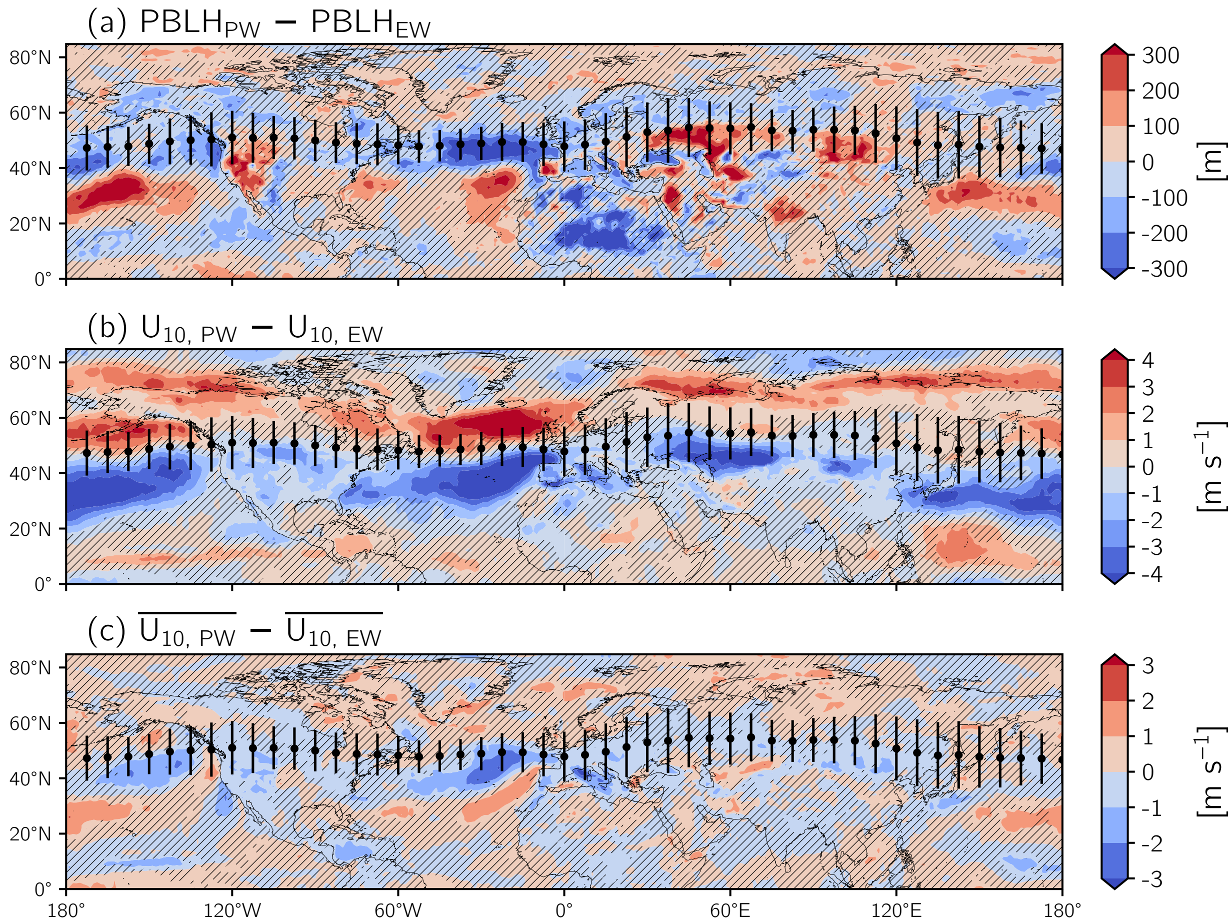

Figure S4. Same as Figure 6 in the main text but for (a) $PBLH$, (b) U_{10}, and (c) $\overline{U_{10}}$.

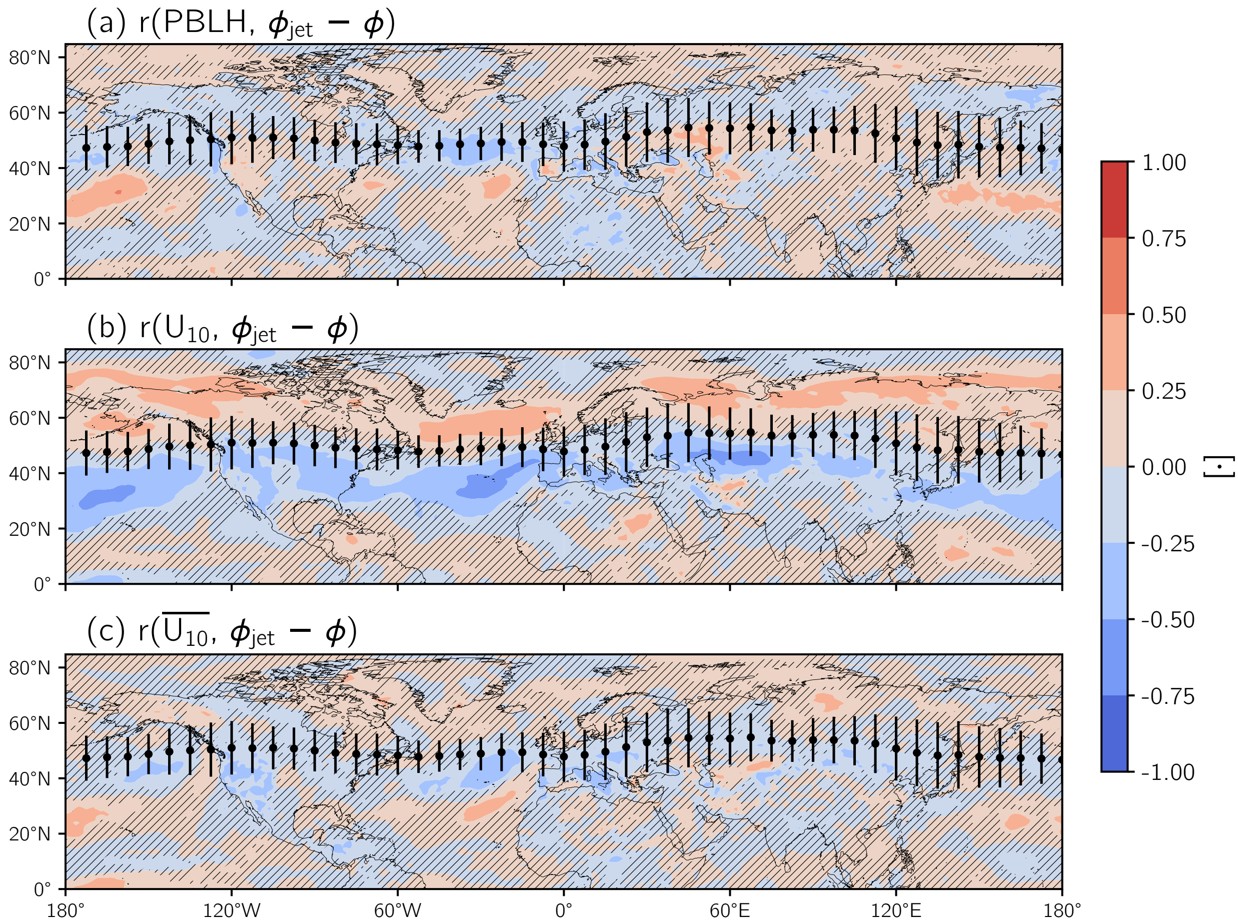

Figure S5. Same as Figure S3 but for (a) $PBLH$, (b) U_{10}, and (c) $\overline{U_{10}}$.

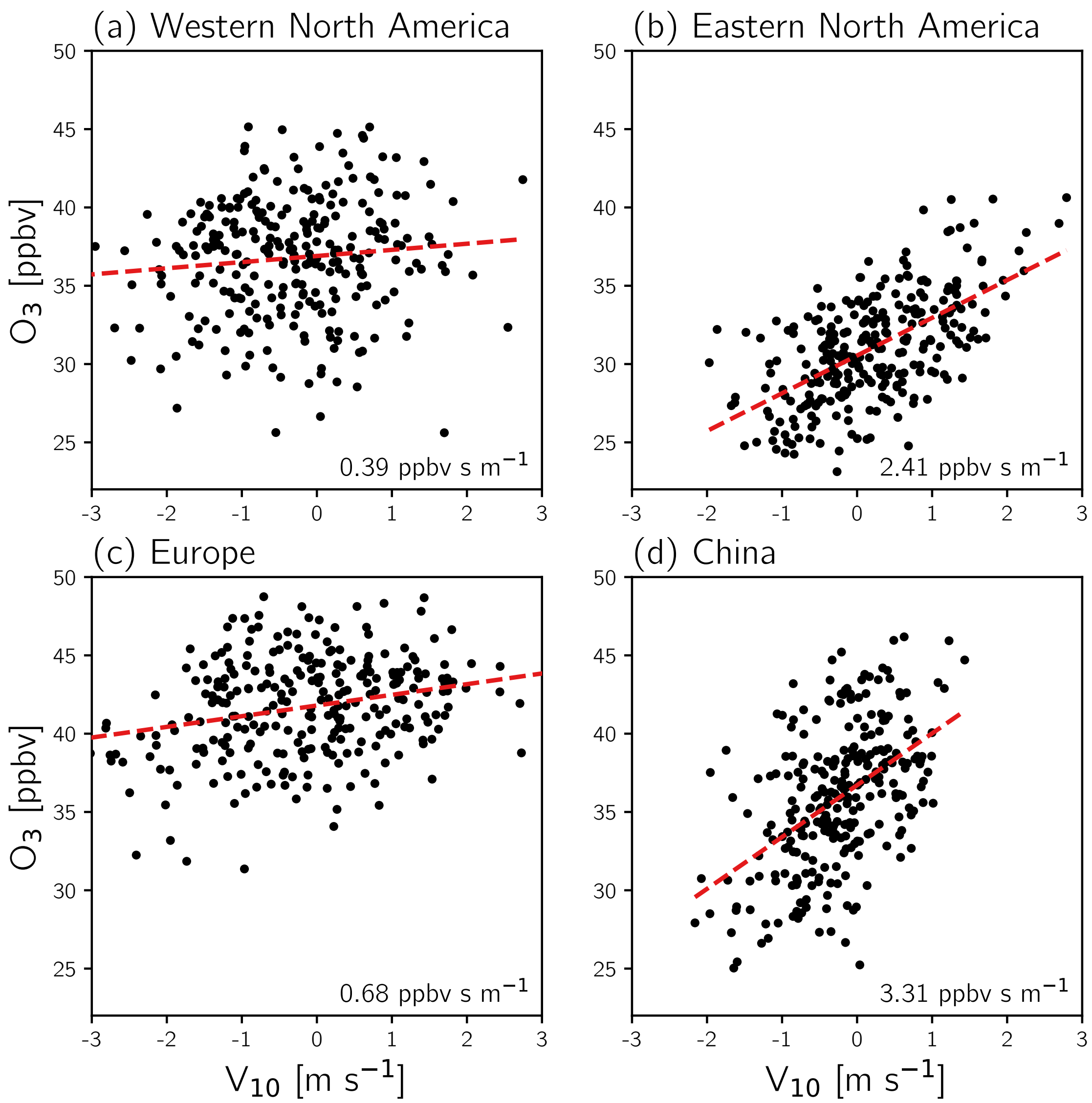

Figure S6. Regionally-averaged O_3 from the control simulation versus regionally-averaged V_{10}. Regional averaging is conducted over the longitudinal extent of the regions listed in each subplots' title but only within ±5° of the mean position of the jet: western North America (125° − 100°W), eastern North America (100° − 65°W), Europe (10°W−30°E), and China (90° − 125°E). Red dashed lines represent the OLS regression, and inset text indicates its slope.